68-14,774

BROTHERS, Alfred Douglas, 1939-

OPTICAL PROPERTIES OF HALIDES OF SILVER AND THALLIUM UNDER HYDROSTATIC PRESSURE.

Iowa State University, Ph.D., 1968
Physics, solid state

University Microfilms, Inc., Ann Arbor, Michigan

OPTICAL PROPERTIES OF HALIDES OF SILVER AND THALLIUM UNDER HYDROSTATIC PRESSURE

by

Alfred Douglas Brothers

A Dissertation Submitted to the
Graduate Faculty in Partial Fulfillment of
The Requirements for the Degree of
DOCTOR OF PHILOSOPHY

Major Subjects: Physics
Education

Approved:

Signature was redacted for privacy.

In Charge of Major Work

Signature was redacted for privacy.

Heads of Major Departments

Signature was redacted for privacy.

Dean of Graduate College

Iowa State University
Ames, Iowa

1968

TABLE OF CONTENTS

INTRODUCTION

The use of hydrostatic pressure, combined with low temperatures, is a valuable technique in the study of crystal properties. Pressure changes the lattice parameter while leaving the vibrational amplitudes of the ions essentially unchanged. This may be contrasted to the effects of changing the temperature of the sample, which alters both the lattice parameter and the vibrational amplitudes of the ions. At low temperatures only the lowest vibrational states of the crystal are excited. This results experimentally in a better resolved and simpler optical spectrum.

In this work the effects of hydrostatic pressure applied to single crystals and thin evaporated films of AgBr, AgCl, TlBr, and TlCl were studied optically at low temperatures. As is well known, insulators have an energy gap, E_g, of a few electron volts (eV) between their valence and conduction bands. Electronic transitions from the valence to the conduction band are stimulated by incident photons of energies near E_g and greater. For the above four materials, this occurs in the visible to near-ultraviolet wavelength region. The shape of this absorption edge and its position with respect to E_g are properties of the band structure of the crystal. The pressure shift of this absorption edge can yield information about the relative changes in the valence and conduction band structures. Similar pressure shifts for the absorption edges

of crystals whose crystal structures are quite similar, which will be shown to be the case for AgBr and AgCl, indicate electronic transitions from valence bands of the same symmetry to conduction bands of the same symmetry.

At incident photon energies generally below those at the beginning of the absorption edge lie absorption peaks caused by the formation of excitons. Excitons may be defined as quanta of non-conducting electronic excitation energy associated with the entire crystal, whose motion through the periodic crystal lattice may be characterized by a wave vector. They may alternately be thought of as a loosely bound electron-hole pair with effective masses m_e^* and m_h^* respectively, separated by a dielectric medium. This describes the very useful Wannier exciton model (1). Discrete exciton energy levels exist immediately below the conduction band. These discrete levels may produce a series of exciton absorption peaks near or superimposed upon the absorption edge.

Thin evaporated films of AgBr, AgCl, TlBr, and TlCl were studied since the exciton absorption peaks occur at much higher levels of absorption than could be measured using thick single crystals. In these films the absorption in the wavelength region of the exciton peaks was sufficiently low so that the desired optical measurements could be made.

There exist several possibilities for the shape and position of the absorption edge, each of which implies a different

exciton absorption spectrum. The momentum which the incoming photons supply to the crystal is negligible compared to the momentum of a typical electron in a crystal. For the case in which the valence band maximum appears directly below the conduction band minimum, the transition is called a direct transition. An electron is raised from the valence band to the conduction band with no change in momentum (or wave vector k). See Figure 1a.

The onset of absorption is depicted by transition 1 between the two extrema. This occurs at the gap energy, E_g. As the transitions occur farther away from the maximum of the valence band, as transitions 2 and 3 in Figure 1a, increasingly greater numbers of electronic states are involved, resulting in the increase of the absorption coefficient, α, as shown in Figure 1b. The shape of the absorption edge varies as $(\hbar\omega - E_g)^{\frac{1}{2}}$ (2) where $\hbar\omega$ is the incident photon energy.

The discrete states arising from the creation of excitons have binding energies, B, of a few hundredths of an eV as measured from the conduction band. Since incoming photons provide essentially no momentum for the electron-hole pairs they create, the transitions are all essentially vertical. Excitons can have net momenta and kinetic energy of motion through the lattice, described by exciton energy bands, shaped similarly to the conduction band, which appear in Figure 1c. Only the states of zero momentum can be reached by absorbing a

DIRECT EDGE
NO ELECTRON-HOLE INTERACTION

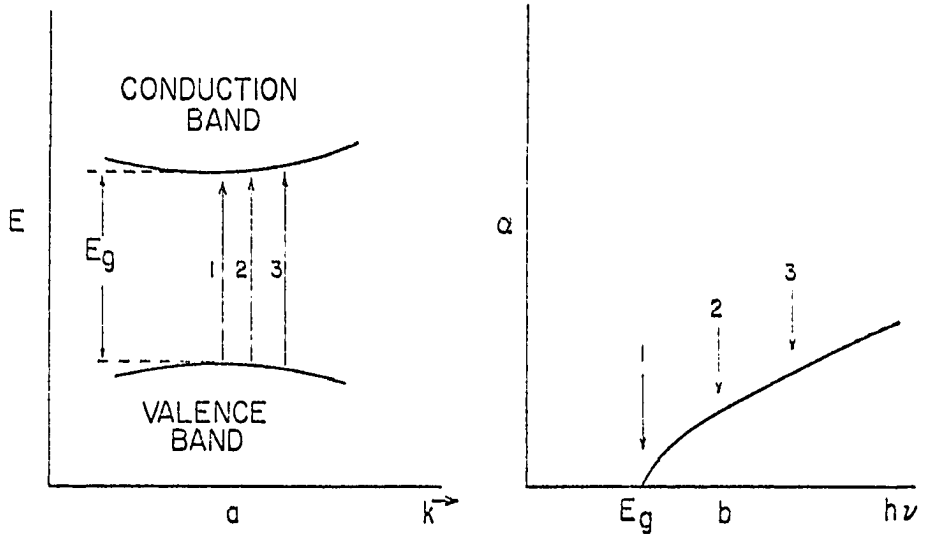

WITH ELECTRON-HOLE INTERACTION

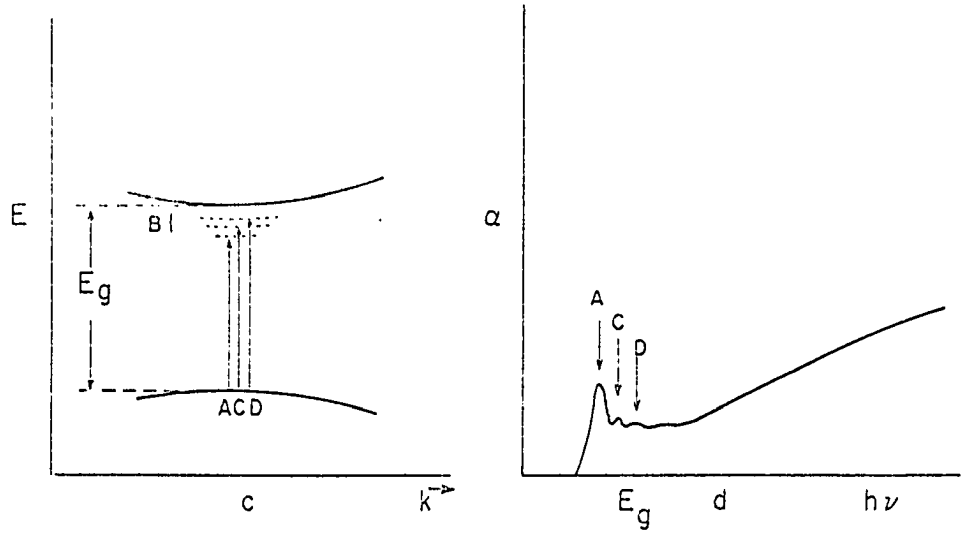

Figure 1. Schematic representation of the direct absorption edge

photon, however. Transitions from the valence band maximum to these levels (A, C, and D in Figure 1c) result in the modified spectrum of the edge as displayed in Figure 1d. Using the Wannier model, the oscillator strengths of the peaks corresponding to transitions A, C, and D vary as n^{-3} where n = 1 represents the lowest discrete energy level, and the oscillator strength of a band may be defined as the integrated area under the absorption band. For this reason often only the absorption peak corresponding to the n = 1 transition is seen experimentally.

The enhancement of the absorption beginning at E_g is due to the creation of electron-hole pairs which remain nearby, since the incident photons here cannot supply energy enough to separate the electron and hole rapidly. This condition increases the value of the matrix elements which determine the intensity of absorption. As the energy in excess of that needed to create the free electron and hole increases, that is, the incident photons become more energetic, this enhancement decreases.

The indirect edge is treated schematically in Figure 2. Here the conduction band minimum and the valence band maximum lie at different values of k. Transition 1 (Figure 2a) occurs with the absorption or emission of a phonon to conserve momentum. The possibility of transitions which absorb or emit phonons adds to the complexity of the indirect absorption

INDIRECT EDGE
NO ELECTRON-HOLE INTERACTION

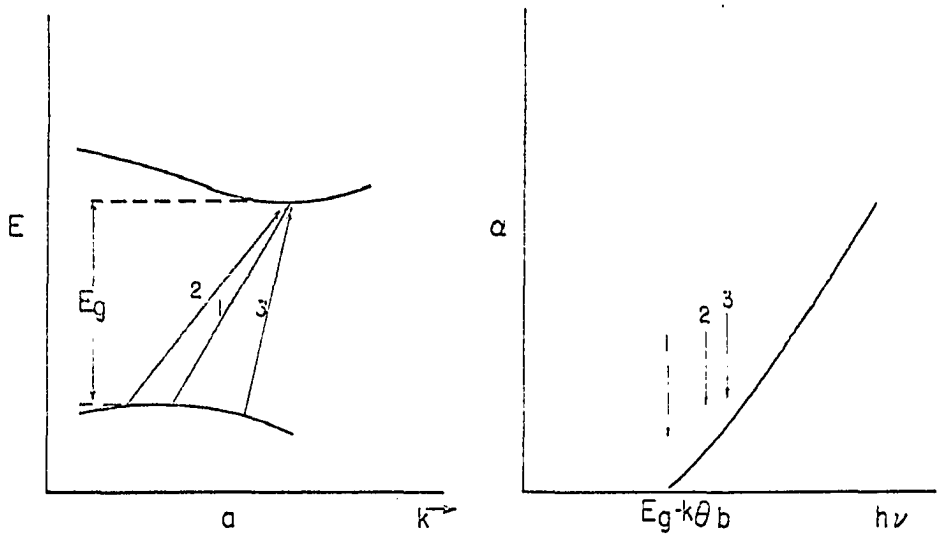

WITH ELECTRON-HOLE INTERACTION

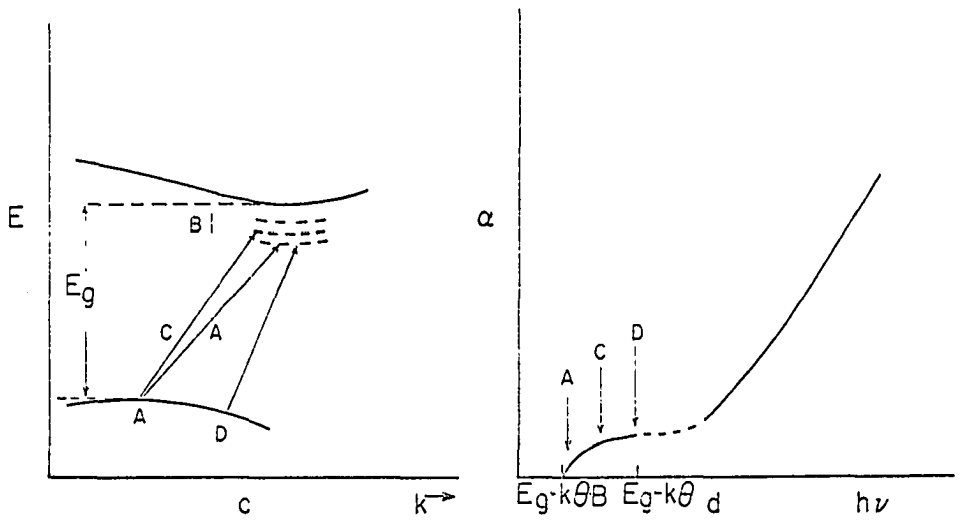

Figure 2. Schematic representation of the indirect absorption edge

edge. The beginning of the absorption edge is at $(E_g - k\theta)$, where $k\theta$ represents a phonon energy of typically a few hundredths of an eV. Transitions such as 2 and 3 also occur, utilizing phonons of different momenta than transition 1. The increase in the number of states farther from the valence band maximum again produces the rise in absorption with increasing incident photon energies. Notice that the functional dependence of the edge here is $(\hbar\omega - E_g \pm k\theta)^2$ (2) compared with $(\hbar\omega - E_g)^{\frac{1}{2}}$ for the direct edge. This suggests that the indirect edge should rise more sharply than the direct edge. The fact that the opposite condition is generally seen points out the importance of the coefficients of these terms, which are not included here.

Introduction of electron-hole interactions again complicates the absorption spectrum. Transitions A and D (Figure 2c) differ not only in the energy change which they effect, but also in the momentum of the phonon needed for the transition. From this it can be seen that a broad range of energies is available for transitions to each exciton energy level. Thus the added absorption component, beginning now at $(E_g - k\theta - B)$, is devoid of sharp peaks (Figure 2d). Another cause of this structureless absorption is that two transitions may occur from the same location on the valence band, yet proceed to different k values on the exciton energy bands. This could create two excitons of similar energies, but very different

momenta, just as transitions A and C create two excitons of comparable momenta but quite different energies.

For either the direct or indirect transitions both allowed and forbidden transitions can occur. Allowed and forbidden are used here in a sense similar to allowed and forbidden transitions in the hydrogen atom problem, governed by angular momentum selection rules.

It should be noted that although the oscillator strengths for excitons are only about 0.1 as compared to 0.8 or better for many defects in a crystal lattice, the exciton absorption peaks can be quite prominent. This is possible because every atom in a crystal is capable of yielding an exciton, compared to perhaps one in ten thousand or more for defects or impurities.

Table 1 (2) contains a summary of the expected functional dependence of the absorption edge and the exciton spectra for all the above-mentioned cases.

Although exciton absorption peaks generally occur at energies below E_g, germanium offers an example of a system in which this absorption occurs at energies greater than E_g (2). The lower energy absorption edge in germanium is an indirect edge at about 0.6 eV. A second edge appears at about 0.8 eV. Associated with this edge is a direct exciton, which, as a result, appears about 0.2 eV above the onset of absorption.

A further complication in the spectra studied in this

Table 1. Summary of the functional dependence of the absorption edge and excitons for direct and indirect transitions

Transition	Energy dependence of optical absorption coefficient κ	
	Exciton effects neglected	Exciton effects included
Direct allowed	$(\hbar\omega - E_0)^{\frac{1}{2}}$	Lines at $\hbar\omega = E_0 - \frac{R}{n^2}, \quad n = 1, 2, 3, \ldots$ $f_n \sim \frac{1}{n^3}$
		For the continuum $K \sim \frac{\exp \pi\alpha}{\sinh \pi\alpha}$, where $\alpha = \sqrt{\frac{R}{\hbar\omega - E_0}}$
Direct forbidden	$(\hbar\omega - E_0)^{\frac{1}{2}}$	Lines at $\hbar\omega = E_0 - \frac{R}{n^2}, \quad n = 2, 3, 4\ldots$ $f_n \sim \frac{n^2-1}{n^5}$
		For the continuum $K \sim \left(1 + \frac{1}{\alpha^2}\right) \frac{\exp \pi\alpha}{\sinh \pi\alpha}$
Indirect allowed components	$(\hbar\omega - E_g \pm k\theta)^2$	Bound excitons $K \sim \frac{1}{n^3}(\hbar\omega - E_g \pm k\theta)^{\frac{1}{2}}, \quad n = 1, 2, 3\ldots$
		For the continuum $K \sim (\hbar\omega - E_g \pm k\theta)^{\frac{1}{2}}$
Indirect forbidden components	$(\hbar\omega - E_g \pm k\theta)^3$	Bound excitons $K \sim \frac{n^2-1}{n^5}(\hbar\omega - E_g \pm k\theta)^{\frac{1}{2}}, \quad n = 2, 3, \ldots$
		For the continuum $K \sim (\hbar\omega - E_g \pm k\theta)^{\frac{3}{2}}$

work arises from the large number of electrons available from both the anions and cations of the four crystals studied. Band structures resulting from so many electrons cannot be expected to be either simple or isotropic in k space. Application of pressure will likely cause a non-uniform distortion of these band structures. Paul (3) has found that different band edges likely have different deformation potentials, which makes pressure experiments valuable in sorting out complicated band structures. The deformation potential may be defined as

$$E_d = \left(\frac{\partial E_g}{\partial \ln V}\right)_T$$

when hydrostatic pressures are used. He also suggested that changes in position and shape of the optical absorption edge can be clues to the presence of different scattering mechanisms, particularly impurity scattering, and of multiple extrema having different pressure coefficients.

The present work was undertaken as an attempt to understand better the band structure of the silver and thallium salts studied. The silver salts have been extensively studied, and calculated band structures which exhibit the known characteristics of the absorption edges and excitons in these salts are available and in general agreement (4,5). Because of the complexity of the silver salt band structures, to be discussed later, the added information obtained here is valuable in sorting out some areas of important, albeit subtle, disagree-

ment in the calculations. Although no similar calculations have been attempted for the thallium salts, several other recent experiments have provided insights into their band structures.

APPARATUS

The pressure generating system (see Figure 3 for a block diagram) was designed to attain pressures up to 10,000 atmospheres using helium gas as the pressure transmitting fluid. The system was charged with helium gas from an auxiliary pressure system which boosted the pressure to about 350 atmospheres from 150 atmospheres out of the tank. This system was then valved off and the pressure regulated as desired with the main system. Because of the reduced dimensions of the pressure cell used in this experiment, a pressure of 3500 atmospheres was judged to be the maximum safe pressure. This limit did not impose severe restrictions on the accuracy of the pressure shifts measured, since most were large even over the limited range available. Thus the intensifier (I Figure 3) and related parts were not used.

The pressure system employed a Southern California Engineering Corporation air driven oil pump capable of producing oil pressures to 4500 atmospheres. This pump was used to drive the piston of the oil-helium separator (S Figure 3). The separator was machined from Allegheny-Ludlum Almar 300 maraging steel and provided with a protective iron sheath pressed over its length. The pressure sealing rings were of standard design, composed of neoprene and lead washers sandwiched between discs of maraging steel and forced against a polished seat by the retaining nuts. The location of the

Figure 3. Block diagram of pressure system used in the experiment

F - Air filter and oiler

P - 0-70,000 psi hydraulic pump

R - Oil reservoir and filter

B_1 - Oil bleed valve

G_1 - 0-75,000 psi Bourdon gauge (oil)

S - Oil-helium separator

I - Harwood A2.5J intensifier

V - 200,000 psi needle valve

T - Oil trap

M - Manganin gauge

B_2 - Helium bleed valve

G_2 - 0-7000 psi Bourdon gauge (helium)

——— indicates 1/4" O.D. x 0.060" I.D. stainless steel tubing

– – – – indicates 3/16" O.D. x 0.020" I.D. stainless steel tubing

——— indicates 1/8" O.D. x 0.020" I.D. stainless steel tubing

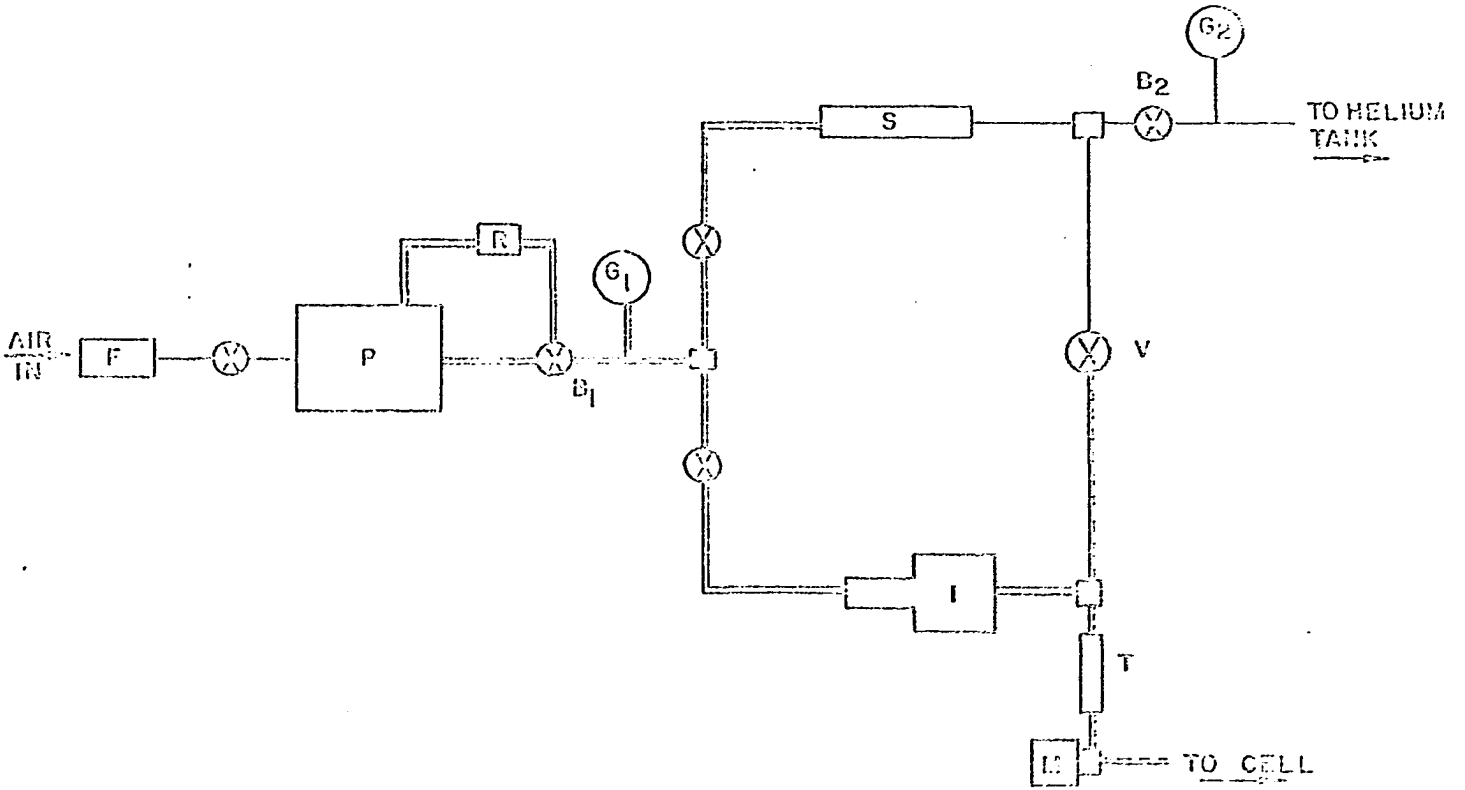
AIR IN
F
P
R
G_1
B_1
S
G_2
B_2
TO HELIUM TANK
V
I
T
M
TO CELL

piston in the separator was monitored using a linear variable differential transformer mounted over a length of 3/8" diameter pressure tubing. Inside the tubing rode a soft iron slug attached by a long non-magnetic rod to the piston. A balancing circuit driven by a servo motor connected to the transformer by a cord kept the transformer centered about the core. The position of the piston could then be determined by the position of a pointer on the servo motor shaft.

Pressure tubing used was 1/8" diameter 60,000 psi test and 3/16" diameter, both with a 0.020" hole. Tubing containing the helium gas was 100,000 psi test stainless steel. The oil lines were 1/4" diameter 60,000 psi test stainless steel. All valves used were 60,000 psi test. As a safety precaution the system was enclosed in a 1/8" steel-plated cart.

The design of the pressure cell (see Figure 4) was a result of several preliminary test models (6) and proved very satisfactory. Made also of maraging steel, it measured 2 5/8" in diameter by 2" high. The sealing surface of the cell body was carefully polished before and after hardening the steel. The "mushroom" plugs (R) are of the unsupported area design (7) and also made of maraging steel. The surfaces onto which the sapphire windows were attached were machined flat, then polished in a vibrating bed polisher with alumina until they appeared smooth when viewed under a microscope. The sapphire windows, oriented with the c-axis perpendicular to the flat

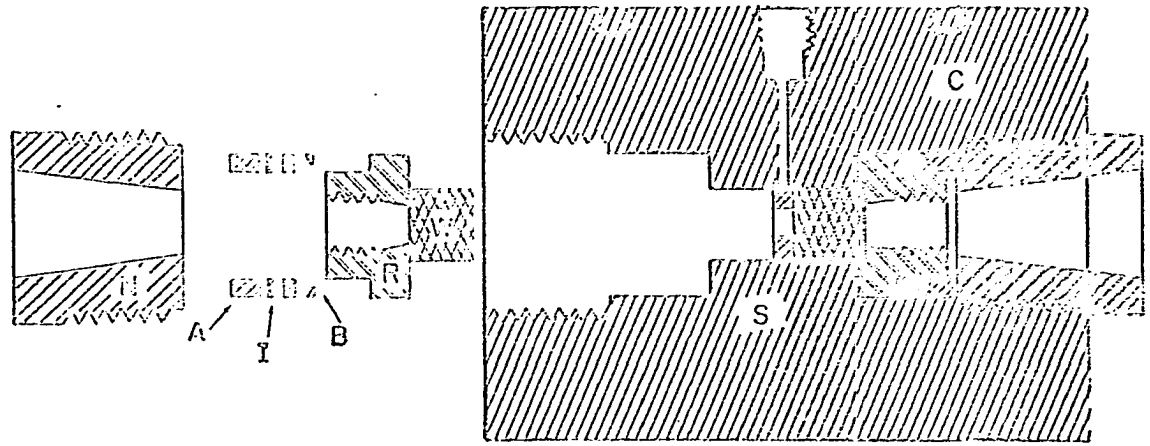

Figure 4. Pressure cell

C - Cell body
N - Retaining nut
R - Pressure seal
W - Sapphire window
S - Sample holder
B - Brass extrusion ring
I - Indium gasket
A - Steel retaining ring

face and flat to within ± 0.0001", were varnished onto the mushroom plugs with General Electric 7031 low temperature varnish. The brass extrusion rings (B) were of triangular cross section and served to prevent the indium sealing ring (I) from extruding and jamming the plug in the cell. The hex-head maraging steel nuts (N) were tightened securely against the retaining ring (A). The optical path was a cone of 16° included angle, with minimum openings of 3/16" at the sapphire window seats.

The cryostat used was a double reservoir, single vacuum jacket container (Figure 5). The pressure cell was bolted to the bottom of the helium reservoir by means of a copper disc which was first bolted to the cell, then this assembly bolted to the cryostat. Pressure was introduced into the cell through a section of the 1/8" tubing described above, running through the center of the cryostat. The tubing was sealed at the top with a compression type O-ring vacuum seal. A spacer was provided to center the tubing in the shaft as well as to lengthen the distance between the portion of the tubing at liquid nitrogen temperature and that at room temperature. The inner radiation shield was kept at the temperature of the liquid in the inner reservoir. The outer shield was held at liquid nitrogen temperature. The quartz windows were waxed into place, since more elaborate seals were too bulky to allow the cryostat to fit into the sample chamber of the Cary 14R

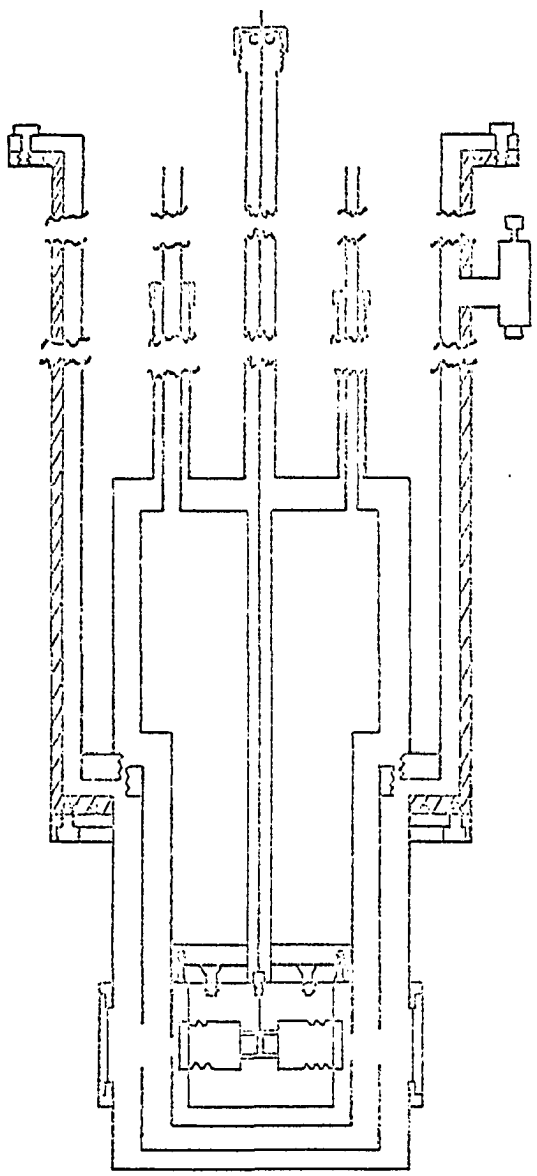

Figure 5. Optical helium cryostat used in pressure experiments

spectrophotometer. The cryostat was machined from stainless steel, except for the outer wall which was aluminum. The cell and the inner reservoir were held in place by the soft solder joints at the inner reservoir vent and fill tubes. These joints were sufficiently sturdy to support the several pounds of the cell, reservoir, and shield, and remained leak tight. The capacity of the inner reservoir was about 2 liters. The cryostat was supported on the spectrophotometer by a rigid stand mounted on the table supporting the spectrophotometer, since the assembly was too heavy to rest directly on the cantilevered sample chamber.

The cryostat used in making the temperature dependence measurements was a Cryonetics single vacuum jacketed cryostat with an exchange gas chamber surrounding the sample chamber. Small amounts of helium exchange gas could be added or removed by a system of valves mounted on the cryostat. Temperatures were measured with a Au-0.02% Fe *versus* Cu thermocouple (8) calibrated carefully to 80°K, with the calibrations extrapolated to 273°K. A heater was provided on the sample holder to allow regulation of the sample temperature.

EXPERIMENTAL

Samples and Sample Preparation

Samples of the single crystals were obtained from various sources. The TlBr and TlCl samples were from the Harshaw Chemical Company. Earlier samples of TlBr and TlCl from Vinor Laboratories not only were colored when received, but gave peculiar results when measured. They were therefore not used. A Vinor AgBr sample was purchased, but it too failed to respond in a believable manner. The AgCl sample and a very pure zone refined AgBr sample were obtained from Dr. R. S. Van Heyningen at the Eastman Kodak Research Laboratory. These yielded spectra which were in excellent agreement with already available results. The crystals were nominally 2 mm thick by 9 mm in diameter when ready for use. Polishing was done on a wax lap using 1 micron and 0.3 micron alumina in water, followed by a few light passes over a facial tissue. The AgCl sample was annealed at 250°C for several hours in a chlorine atmosphere to remove colloidal silver deposits present. The crystals were exposed only to light from Kodak Wratten 1A filters while polishing and loading into the cryostats.

The thin film samples were made from reagent grade chemicals evaporated onto quartz substrates. These substrates were carefully cleaned prior to the evaporations by first scrubbing with an alcoholic KOH solution, then rinsing with solvents and distilled water until the water covered the

quartz in an even layer. The substrates were then dried with a stream of hot air and loaded immediately into the evaporator. A 25 mm^2 quartz plate was placed next to the sample substrate. The square quartz rested on a stainless steel support which masked a strip about 2 mm wide across the center. After the evaporation this mask was removed and the whole square overcoated with a layer of silver by evaporation. These were used to make thickness measurements of the samples.

The evaporator was composed of a 7" diameter pyrex bell jar using a teflon seal. Pumping was done by two 4 liter per second Varian vacion pumps after the system was roughed out. Typical evaporation pressures were 10^{-5} Torr, with a sample to substrate path length of about 10 cm, considerably smaller than the mean free path of the evaporating molecules. Evaporations were made as rapidly as was consistent with the above-mentioned pressure limit. To prevent spattering of the silver salts while evaporating, a closed tantalum cylinder with two small holes pointed in the general direction of the sample was used. Evaporations of the thallium salts went smoothly and rapidly directly from the tantalum boat. Due to the low evaporation temperatures of all these salts, outgassing of the sample before evaporation was not feasible.

Thickness measurements were initially made on a spectrometer modified and calibrated by Mr. R. M. Morgan. Interference effects which arose from bringing the silver overcoated sample substrate in contact with a half silvered reference

mirror provided the means of measuring the thickness (9, p. 105). Later a Varian multiple beam interferometer was obtained, whose accuracy was reported to be $\pm$ 30 Å. Checks between the modified spectrometer and the Varian interferometer indicated that the spectrometer was well calibrated, although somewhat less accurate than the interferometer.

Special care was again taken to prevent white light from striking the films. The silver halide films clouded immediately on exposure to white light. The evaporator was shrouded before and after the evaporation, and the evaporation was performed in a dark-room. The films were handled under light from Kodak Wratten 1A filters. The films were generally placed in the cryostat immediately after they were produced.

Procedure

The crystals were studied as follows. The pressure sealing windows were varnished onto the mushroom plugs. After at least several hours of drying time, the excess varnish was removed from the optical path of the plug assembly. The sample was then placed in the pressure cell, this mounted in the cryostat, and the cryostat evacuated. The initial pressure had to be about 1000 atmospheres to prevent helium leakage through the varnish seals when they were cooled. The cryostat was then cooled by placing liquid nitrogen in both reservoirs. After about three hours, the pressure was increased to the maximum desired value, usually about 3000

atmospheres. The liquid nitrogen was blown out of the inner reservoir and the helium transfer begun. Unfortunately there was no way to introduce a thermocouple into the sample chamber of the pressure cell. A thermocouple attached to the copper mounting disc or to the exterior of the cell was of little value, since these areas are the first to cool. The transfer was made slowly, usually over a period of 40 minutes. This was done to allow the cool helium gas to cool the sample most effectively as well as to insure an ample amount of helium in the reservoir when the transfer was over, since the cell took a considerable length of time to cool to an equilibrium temperature. During the runs the vacuum pumping system, consisting of a forepump and an oil diffusion pump, was left connected in case a minor pressure leak might occur.

Helium solidifies at 20-30°K at these elevated pressures. It was assumed that solidification would begin first at the region where the mounting plate and the pressure tubing outlet were located. If this were the case, which is most likely, the pressure in the trapped volume of the sample chamber would drop in accordance with the pressure vs. temperature diagram of solid helium (10). For pressures near 3000 atmospheres a pressure drop of 8% upon solidification was estimated from this curve. The slight decrease in pressure upon cooling to nitrogen temperature was automatically accounted for by reading the pressure as the helium transfer began. Judging from

the fact that the optical densities before and after transfer were essentially the same, and the fact that the sample nearly fills the optical path through the sample chamber, no ill optical effects due to the change of state of the helium were to be expected.

The cryostat was left in place after the spectrum was measured. After warming to near room temperature overnight, the sample chamber was brought to room pressure. The varnish would fail at this low pressure and the remaining helium would enter the vacuum jacket and be removed by the pump. This procedure, in effect, extended the available pressure range by 1000 atmospheres and also insured that no difficulties would appear with the pressure seals after they had been once cycled to liquid helium temperature. The pressure tubing was sealed off at the top of the cryostat to limit the volume of gas to be pumped out before recooling. After the vacuum had recovered, the same cooling procedure as above was used to run another spectrum at zero atmospheres and 10°K.

Because the absorption edges are temperature dependent and no thermocouple could be installed to assess the actual temperature of the sample, the best procedure to attain a reproducible temperature was to allow the pressure cell to come to some equilibrium temperature. Careful account was kept of the time elapsed from the beginning of the helium transfer, and this was used as another method of obtaining

reproducible temperatures, especially when the helium boiled away before an equilibrium temperature was thought to be reached. This problem arose only for the AgCl runs, where the spectra were taken one hour after the transfer began. For the other three salts the times of the measurement were three hours after the transfer began. It was felt that equilibrium had been reached at those times. Since the helium usually remained for up to seven hours after transferring, it was felt that not only had an equilibrium temperature been reached, but that this temperature was quite near liquid helium temperature.

By comparison of the position of the TlCl crystal absorption edge obtained at zero atmospheres to the position of those absorption edges made for the determination of the temperature dependence of the same TlCl single crystal, the sample temperature in the pressure cell after three hours of cooling with liquid helium could be determined to be 10°K, to the nearest degree.

The procedure for measuring the pressure shifts of the peaks of the excitons in thin films was somewhat different, since these spectra were made only at liquid nitrogen temperature. Again the cryostat was cooled for at least three hours prior to the experiment, allowing the cell to come to an equilibrium temperature. The minimum pressure used was again about 1000 atmospheres. Spectra were taken in increments of

about 300 atmospheres to the maximum pressure desired, which was usually about 3400 atmospheres. As a check to determine the extent of any irreversible strains, or a shift in temperature while the experiment was progressing, spectra were taken at descending pressures to 1000 atmospheres as well. In all cases there appeared to be little or no hysteresis in the curves obtained.

This fact, as well as the fact that the exciton peaks sharpened at lower temperatures, was especially encouraging since there was some concern about strains introduced both through differential thermal contraction and pressure induced strains. A further check was made to determine the influence of the differential contraction of the sample and substrate. The table below displays the results of evaporating TlCl onto various substrates.

Table 2. Comparison of pressure shifts of the exciton peaks in TlCl films evaporated onto various substrates

Substrate	Coefficient of linear expansion (α) x $10^{-6}/^{o}C$[a]	Pressure shift of exciton peak x 10^{-6} eV/atm[b]
TlCl	53[c]	--
NaCl	40[d]	-15.8
Fused quartz	0.5[c]	-14.1
Sapphire window	5[c]	-7.8

[a]Room temperature values.

[b]Data taken at liquid nitrogen temperature.

[c]Reference 11.

[d]Reference 12.

Variations in film thickness from 400 Å to 4000 Å affected the pressure shift by only about 10% for any given exciton peak studied. Thus the differences shown in the shifts are thought to be due mainly to the various degrees of adhesion of the sample to the substrate.

Although the fused quartz has a thermal expansion coefficient over two orders of magnitude different from that of TlCl, the measured pressure shift is only about 10% different from the value obtained with a NaCl substrate, which has a thermal expansion coefficient similar to that of TlCl. The TlCl film apparently adhered rather well to the sapphire, which lowered the pressure shift by a factor of two. All values of the exciton pressure shifts later reported will be from films on quartz substrates.

Previous work here by Mr. R. Sealock indicated that AgCl films evaporated onto NaCl and LiF substrates exhibited exciton bands which broadened greatly upon cooling to liquid nitrogen temperature. This broadening was attributed to strains caused by differential contraction between the sample and substrate. The exciton bands in the films studied in this experiment all sharpened upon cooling, further evidence that the films adhered rather poorly to the substrates.

Since cooling 300 Kelvin degrees causes about the same amount of strain from differential contraction as applying 3500 atmospheres of pressure causes strain from differential

compressibility, a broadening of the exciton peaks with increased pressure would be expected if the film adhered well to the substrate. Zallen (13) found this to be true for pure silver films evaporated onto quartz and sapphire compared to an unsupported silver film, as evidenced by greatly varying pressure shifts of the peaks in transmission of the films. Some broadening of the exciton peaks generally did occur in the present experiment. Since the exciton peaks are superimposed on the absorption edges, however, the fractional change in height of the peaks could not accurately be determined, although it was clearly small. The extent of the distortion introduced by differential compressibility of the sample and substrate was felt to be minor not only because the broadening was slight, but also because the films did not adhere to the substrate as well as pure silver adheres to quartz.

The spectra were measured on a Cary 14R spectrophotometer. For all wavelengths greater than 3000 Å a 650 watt accessory quartz-iodine lamp was used. Below 3000 Å the standard Cary hydrogen lamp was used. The spectra of both the exciton peak shifts and crystal edge shifts were taken at the fastest chart speed (5 in./min.) and slowest wavelength drive ($\frac{1}{8}$Å/sec) to provide maximum accuracy in reading the data. The spectrophotometer was equipped with a 0 to 2 optical density (o.d.) slidewire, where

$$\text{o.d.} = \ln \frac{I_o}{I} ,$$

I_o being the reference beam intensity and I the sample beam intensity.

Typical resolution for the thinner films was 4 Å, and for the thicker films about 10 Å. In all cases for the absorption edge pressure and temperature shifts the resolution was better than 4 Å. A calibration of the spectrophotometer in the region of concern indicated that it was off only from +1 Å to +4 Å.

Due to the large number of reflecting surfaces (the cryostat windows, pressure cell windows, and sample) and the high refractive indices of the sapphire and the samples, as well as the greatly decreased beam dimensions in passing through the pressure cell, background optical densities of around one were common. To compensate for this neutral density screens were placed in the I_o beam. The slit height was lowered to its minimum value (8 mm), and the slidewire balance control adjusted to yield a value near zero so that the full range of 0 to 2 o.d. units could be utilized. The background optical densities for the temperature measurements were somewhat lower, around 0.5 o.d. units, since the beam was not as constricted as when it passed through the pressure cell. The assembled cryostat, less sample, was placed in the usual configuration on the spectrometer and a baseline run. This baseline proved to be constant enough to neglect its effect on the spectra measured.

The temperature dependence of the absorption edge in TlCl and TlBr was measured from near liquid helium temperature to near dry ice temperature. The samples were precooled to liquid nitrogen temperature. A spectrum was run at this point for later comparison. The helium transfer was then made and sufficient exchange gas introduced into the sample chamber to bring the pressure to about 50 microns of Hg. This approximate pressure was maintained throughout the experiment by removing or adding small amounts of gas as needed. This substantial amount of exchange gas provided rapid and even cooling in the sample chamber, insuring that the temperature read by the thermocouple, which was attached to the aluminum sampleholder near the sample, was representative of the sample temperature.

A few minutes were usually allowed at each temperature for an equilibrium to be established. The heater was used to bring the sampleholder and sample to successively higher temperatures. When moderate heat had to be introduced this way, more exchange gas was removed and the heat input reduced to obtain better temperature uniformity. After the nitrogen had boiled away in the inner reservoir this method could be used to raise the sample temperature to over 200°K with considerably less than 1 watt input. Again the spectrophotometer was run to obtain the maximum readout accuracy.

RESULTS

Pressure Dependence of Single Crystal Absorption Edges

Figure 6 displays the results obtained when the absorption edge of a AgBr crystal was measured at 10°K. The crosses represent data taken at 2100 atmospheres, while the circles represent data taken at zero atmospheres. The points at the extreme lower left of Figure 6 were obtained from the data by finding the point where the slope of the edge leveled off. This was easily found directly from the strip chart recording. For ordinates greater than 1.4, the points lie on a straight line which connects them to the respective zero ordinate points when extrapolated. The portions of the spectra above these extrapolated lines are redrawn along the baseline of the graph. Notice that the area above the extrapolated straight line seems to be greater at the higher pressure. The horizontal distance between the two straight lines gives the pressure shift of the onset of the crystal's absorption edge, -1.9×10^{-6} eV/atm. The negative sign indicates a shift to lower energy with increasing pressure.

The baseline zero was taken at the point where the o.d. due to the absorption edge appeared to nearly level off. Although the spectrum continued to slope quite gradually toward longer wavelengths, this method of fixing the zero of the baseline introduced little or no error in the results. This conclusion was reached after the pressure shifts found

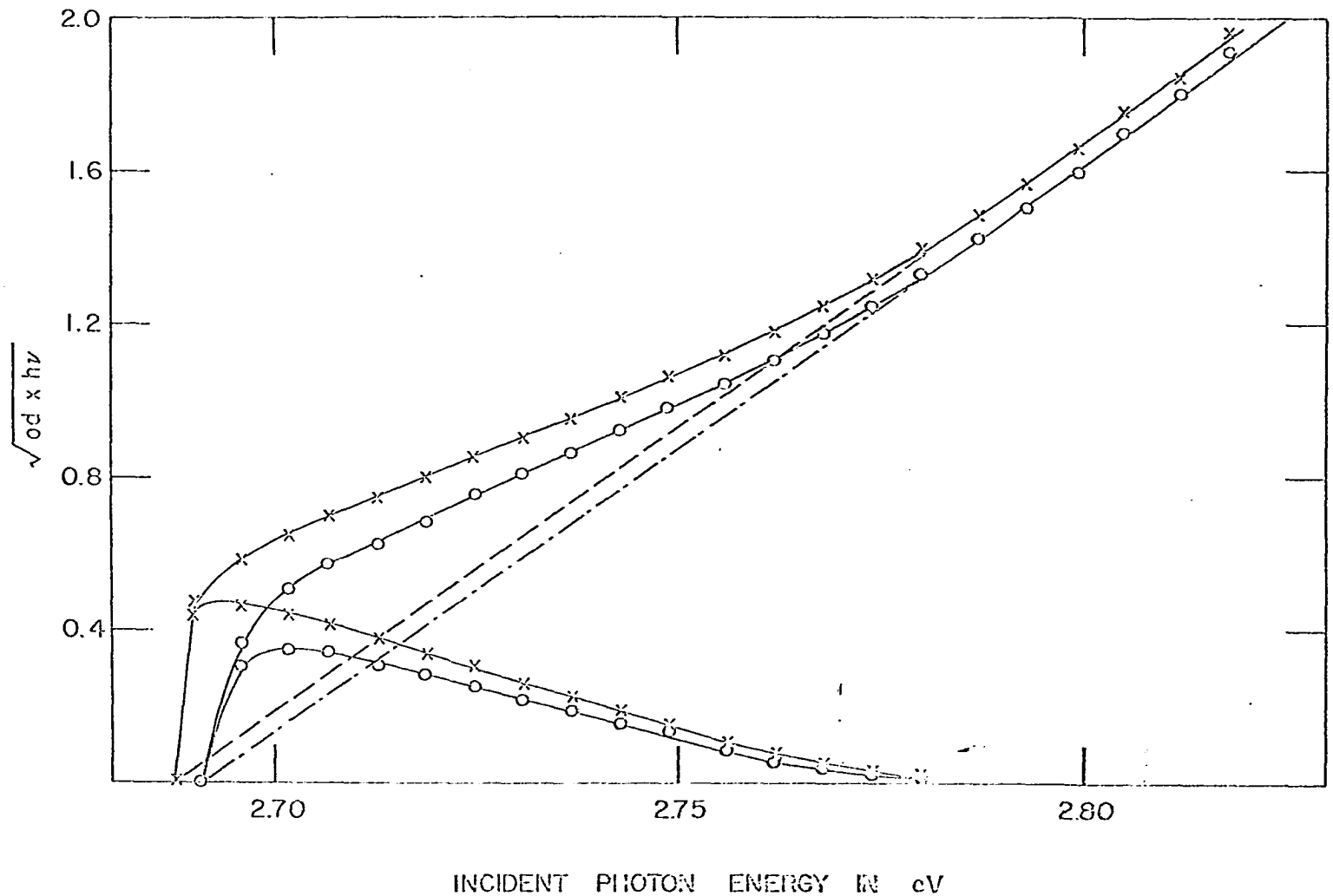

Figure 6. Absorption edge of a AgBr single crystal at 10°K at 2100 atm. (x) and 0 atm (o)

by plotting the data in the above manner were compared to those plotted using the minimum value of the o.d., reached near 0.6 microns as a baseline, as well as those whose baselines were shifted an arbitrary amount as a test of the correctness of the procedure.

The data in Figure 7 display the shape of the AgCl absorption edge at 1830 atmospheres (crosses) and zero atmospheres (circles). The pressure shift of onset of the edge was found to be -1.5×10^{-6} eV/atm. This value was used since the curves tend to merge at higher absorption, indicating that some competing absorption processes may be occurring. The points at the zero ordinate were again easily obtained. Notice that here rather than an enhancement of the edge over a straight line extrapolated from higher o.d., there is a marked dropoff near the beginning of the absorption edge.

The data in Figures 6 and 7 were scaled to compare with those of Brown (14,15) who has studied extensively the optical absorption of these salts. Brown plotted curves obtained from the spectra of several crystals of widely varied thicknesses, so that the present data correspond to only the lower values of $(\alpha h\nu)^{\frac{1}{2}}$ which he plots. The spectrum for the AgBr absorption edge from Brown (14, Figure 8, p. 2372) and the spectrum from the present work (Figure 6, 0 atmospheres) were compared graphically. The values obtained for the onset of the

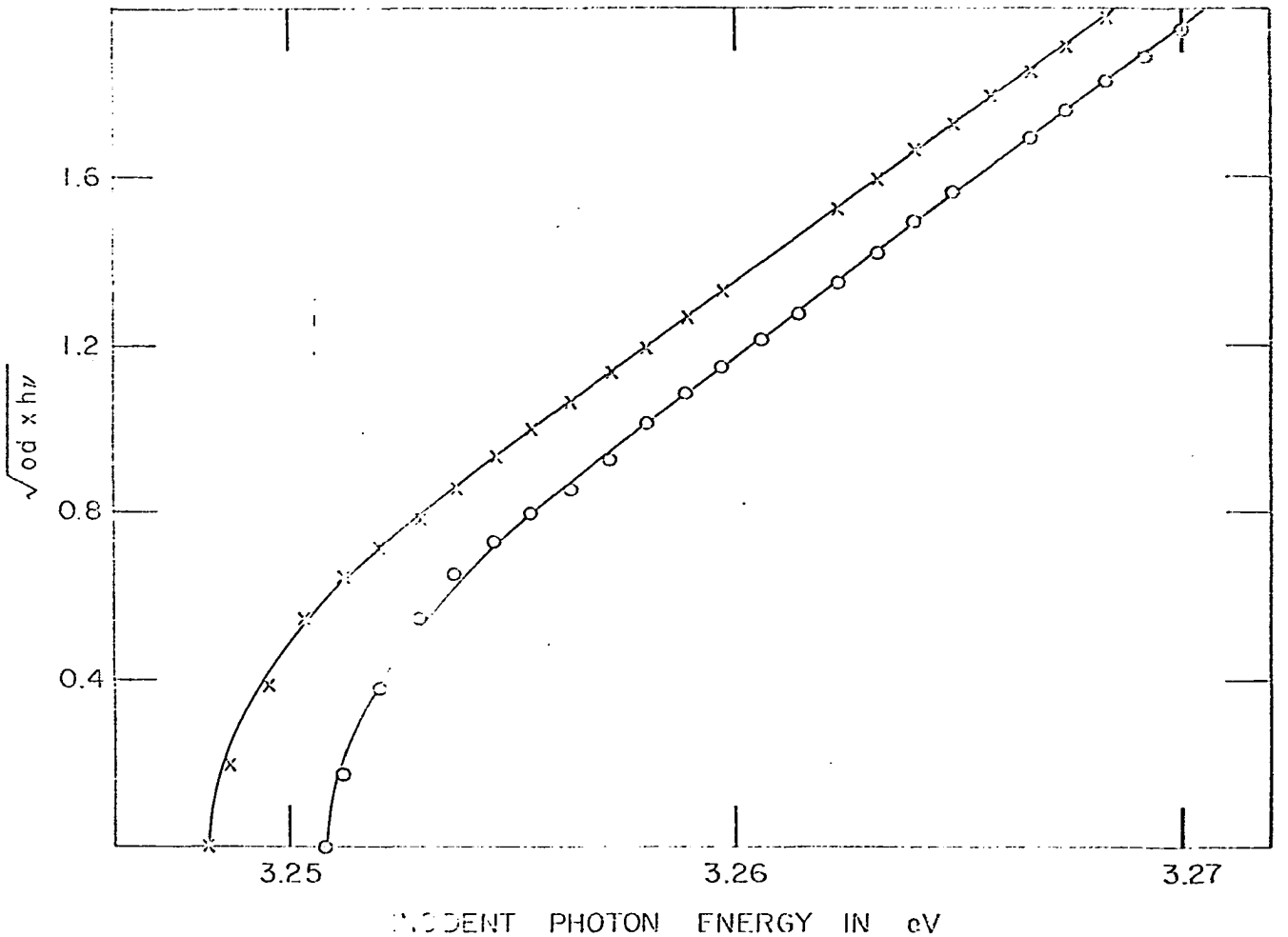

Figure 7. Absorption edge of a AgCl single crystal at 10°K at 1630 atm (x) and 0 atm (o)

absorption edge were 2.690 eV and 2.688 eV respectively. This difference of 0.002 eV was the maximum discrepancy between the two spectra at any point.

When the curve in Figure 7 (0 atmospheres) was compared to those of Brown (14, Figure 9, p. 2373) for the AgCl absorption edge, they were found to possess the same general shape and slope. Although the curve from this work lay generally 0.004 eV to lower energies than Brown's curve at 4.2°K, part of this small discrepancy is attributable to the higher temperature of the sample in this experiment (10°K). Also Brown detected at optical densities less than 0.01 a nearly horizontal foot extending about 0.005 eV to lower energy on the absorption edge. This was not seen in this work because of the very small absorption level as well as the somewhat poorer resolution than Brown had.

The two spectra for TlBr (Figure 8) appear more like those for AgBr than those for AgCl. The crosses represent data taken at 1890 atmospheres; the circles represent data taken at zero atmospheres. The value of the pressure shift of the onset of the absorption edge was found to be -18×10^{-6} eV/atm. Again this value was taken at the onset of the steep absorption component. The curves again tend to merge at higher o.d. Notice that the enhancement found here is of the general shape of that found for AgBr, but smaller. Also it is not clear that one curve is more greatly enhanced than the other.

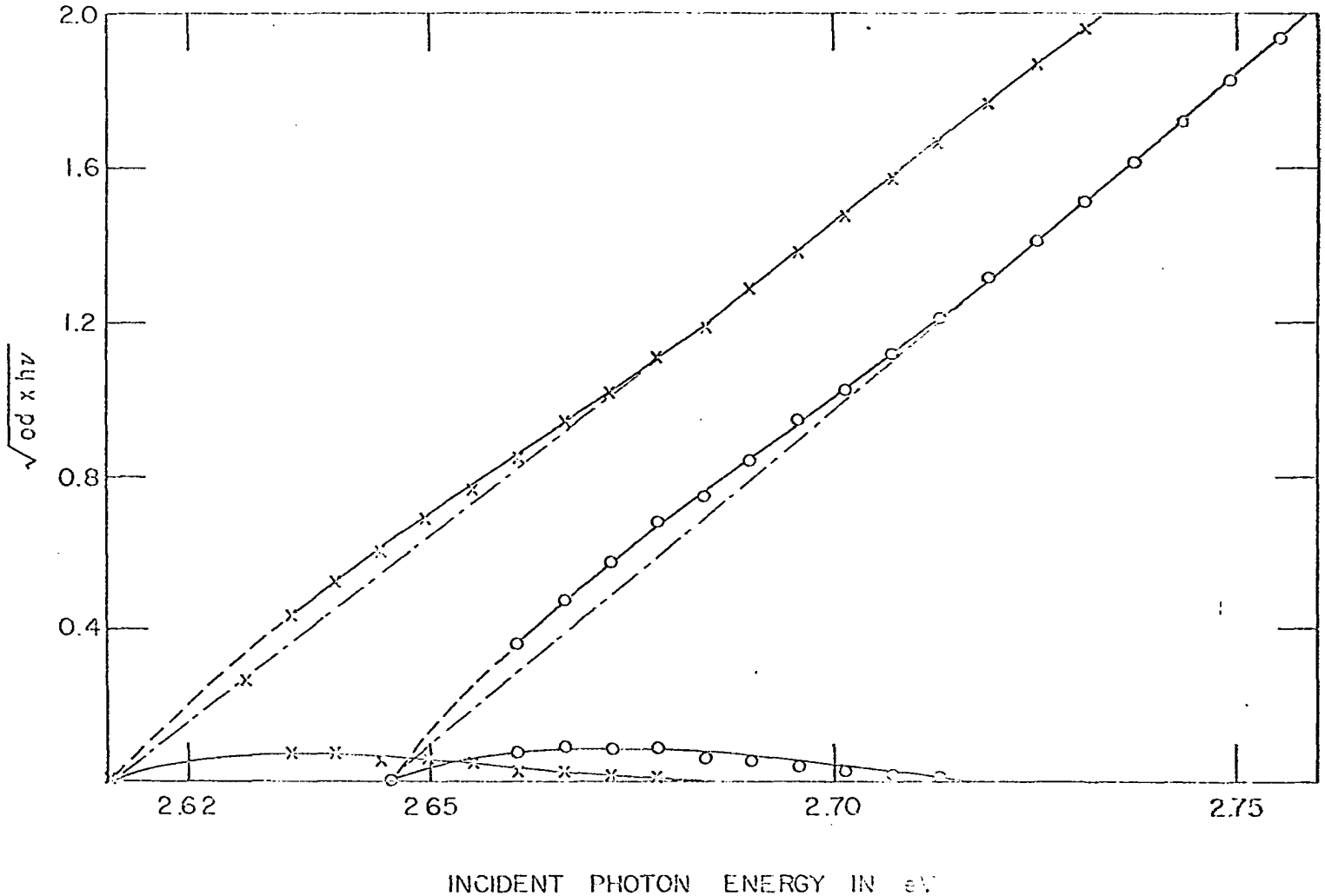

Figure 8. Absorption edge of a TlBr single crystal at 10°K at 1890 atm (x) and 0 atm (o)

Figure 9 gives the absorption edges for a single crystal of TlCl at 1970 atmospheres and zero atmospheres. The value of the pressure shift of the absorption edge as measured at the onset of absorption is -16×10^{-6} eV/atm. Again the curves tend to merge at higher o.d. The shoulders near the beginning of the edges do not appear to be similar to those in TlBr and AgBr. A straight line extrapolation from high o.d. falls far to the high energy side of the horizontal intercept of the curves, rather than nearly through the data points at the horizontal intercepts.

In Figure 10 a comparison of the edges of the four single crystal samples is made. The plots are the zero atmosphere runs of the four preceding figures whose horizontal intercepts have been shifted such that all the absorption edges begin at the incident photon energy E_o. The ordinate could have been expressed equivalently in terms of the absorption coefficient, α, since the crystals all were of comparable thicknesses. In that case the equivalent values of α would range from zero to about 10 cm^{-1}.

The ordinate plotted for the above figures, $(\text{o.d.} \times h\nu)^{\frac{1}{2}}$, is equivalent to $(\alpha h\nu)^{\frac{1}{2}}$ since the reflectivities of the samples used here are small. Plots of the incident photon energy vs. $(\text{o.d.} \times h\nu)^{1/3}$, $(\text{o.d.} \times h\nu)^{2/3}$, $(\text{o.d.} \times h\nu)$, and (o.d.) were made to determine the best functional dependence for the experimental points. These plots have been

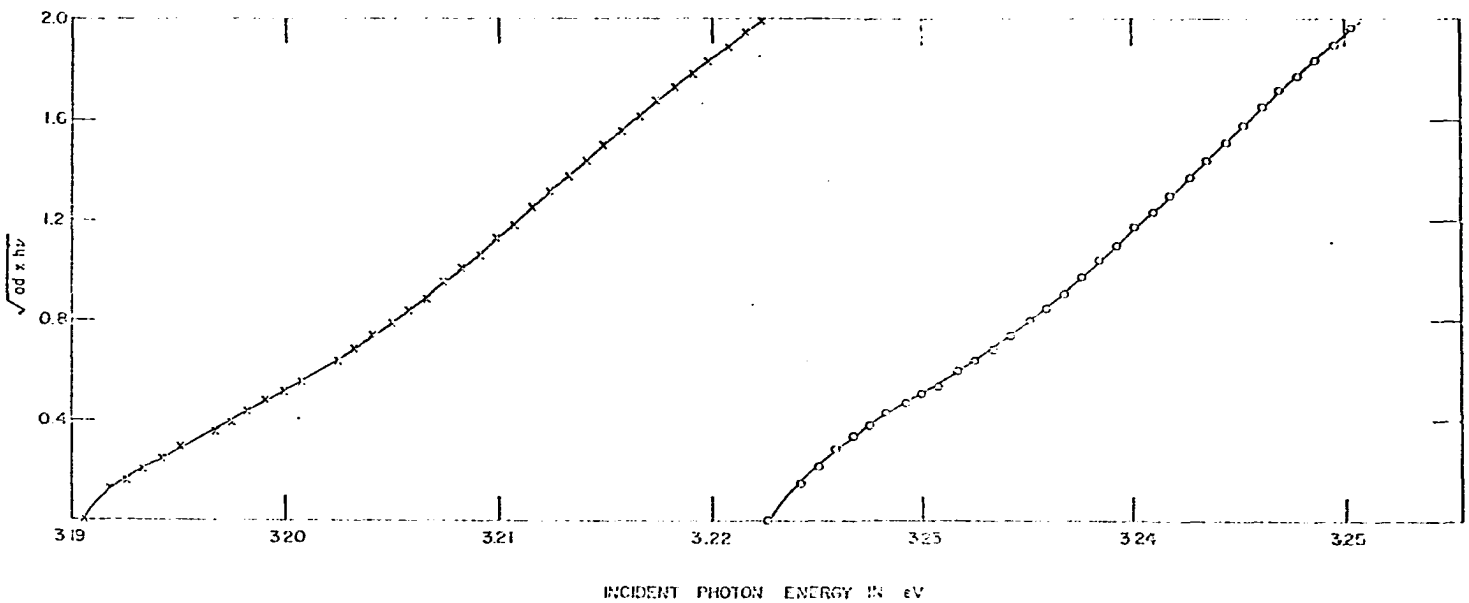

Figure 9. Absorption edge of a TlCl single crystal at 10°K at 1970 atm (x) and 0 atm (o)

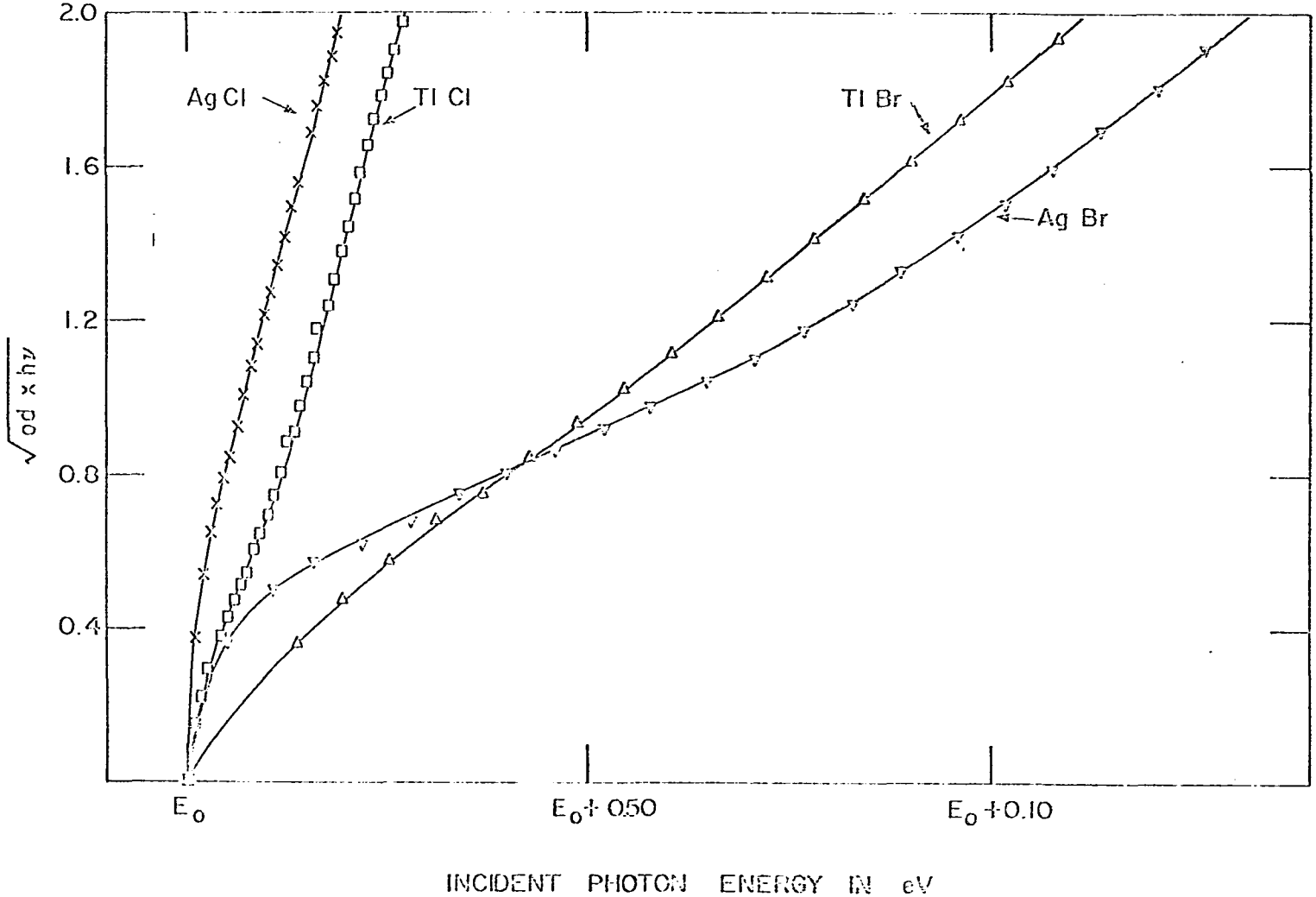

Figure 10. Comparison of the absorption edges of AgBr, AgCl, TlBr, and TlCl single crystals

suggested by other theories (16, p. 202). Another possibility for the functional dependence of the ordinate was suggested by Urbach (17). According to Urbach's rule, the optical absorption increases exponentially with energy near the absorption edge. The data comprising Figures 6 through 10 were plotted in this manner and fit a straight line well. In addition, the values of the pressure shifts obtained from the Urbach rule-plots agree quite closely with those plotted using $(o.d. \times h\nu)^{\frac{1}{2}}$ as the ordinate. Only the Urbach rule plot and the $(o.d. \times h\nu)^{\frac{1}{2}}$ plot did not deviate significantly from a straight line.

Pressure Dependence of Exciton Peaks in Thin Evaporated Films

The pressure shifts of the two observed exciton peaks in AgBr are shown in Figure 11. The peak labeled A lies at about 2600 Å and appears as an unresolved hump in the absorption spectra of very thin films. Peak B is found at about 2900 Å. The spectra were measured at liquid nitrogen temperature. The peak position was arrived at by graphically determining the maximum of the peak for at least two, and usually three, traces of the region including the peak for each pressure attained. A least squares fit was not used since the number of experimental points was small and fell nearly on a straight line. A visual best fit method provided ample accuracy. In this and the following thin films, the films of each of the four types studied whose thickness was most near 1000 Å were

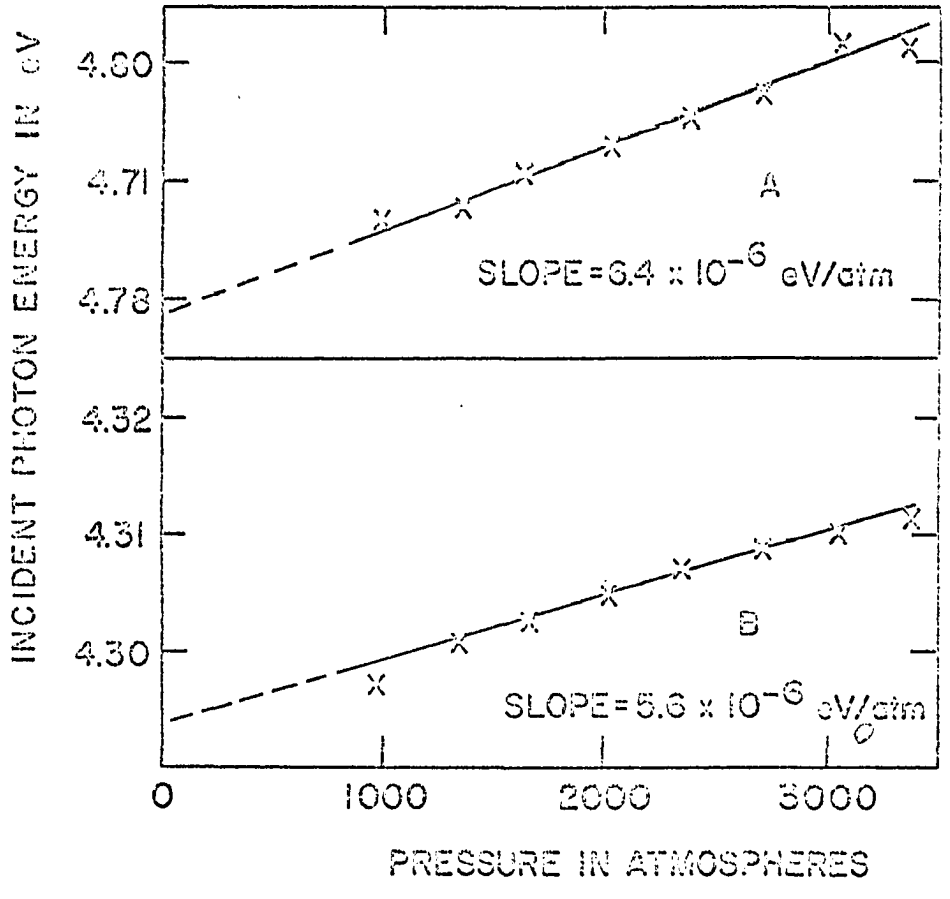

Figure 11. Typical pressure shifts of exciton peaks in AgBr thin films

used as examples of the results.

The slope in Figure 12 gives the pressure shift of the exciton peak in a typical AgCl film studied. Figure 13 displays a typical run from a TlBr thin film, while the pressure shift of the exciton peak in a TlCl thin film is shown in Figure 14. Notice the large negative slopes in Figures 13 and 14 compared with the smaller, positive slopes in Figures 11 and 12.

Temperature Dependence of the Exciton Peak Position in Thin Films of TlBr and TlCl

Figure 15 displays the temperature dependence of the exciton peak in a 1360 Å film of TlBr. The ordinate represents the energy of the exciton peak, obtained in the same manner as described for the exciton peak pressure shifts. Notice that the slope changes sign at about 55°K. Figure 16 shows a typical temperature dependence curve for the exciton peak in a thin film of TlCl. Here the change of slope occurs at about 160°K. It is apparent in both of the above figures that neither curve can be fitted to a straight line at temperatures below 300°K; however it seems reasonable to place an upper limit for the value of the slope of both curves near room temperature as 1×10^{-4} eV/°K.

The temperature dependence of a point near the onset of the absorption edge for single crystals of both TlBr and TlCl was also measured. These curves were of the same general

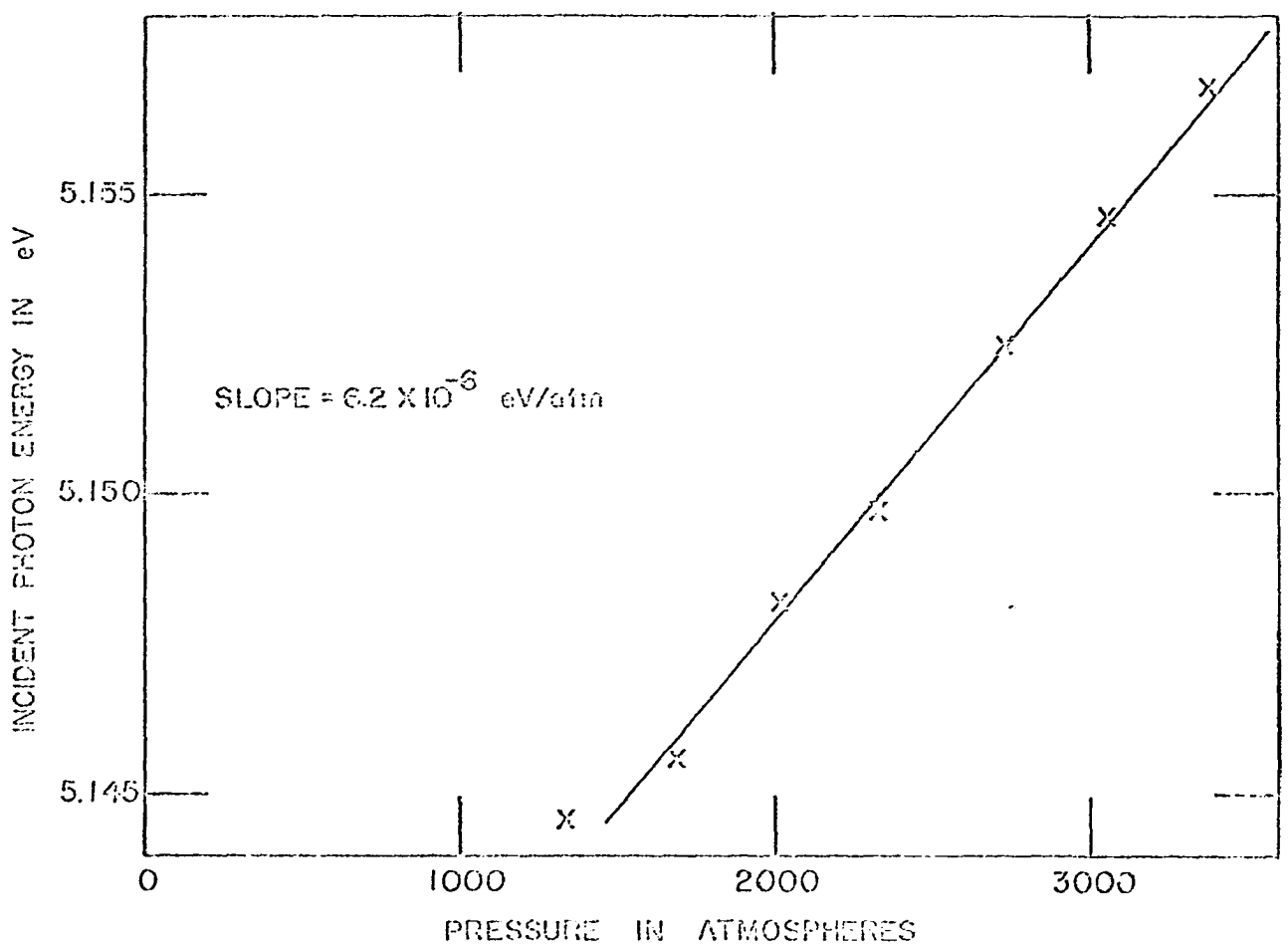

Figure 12. Typical pressure shift of the observed exciton peak in AgCl thin films

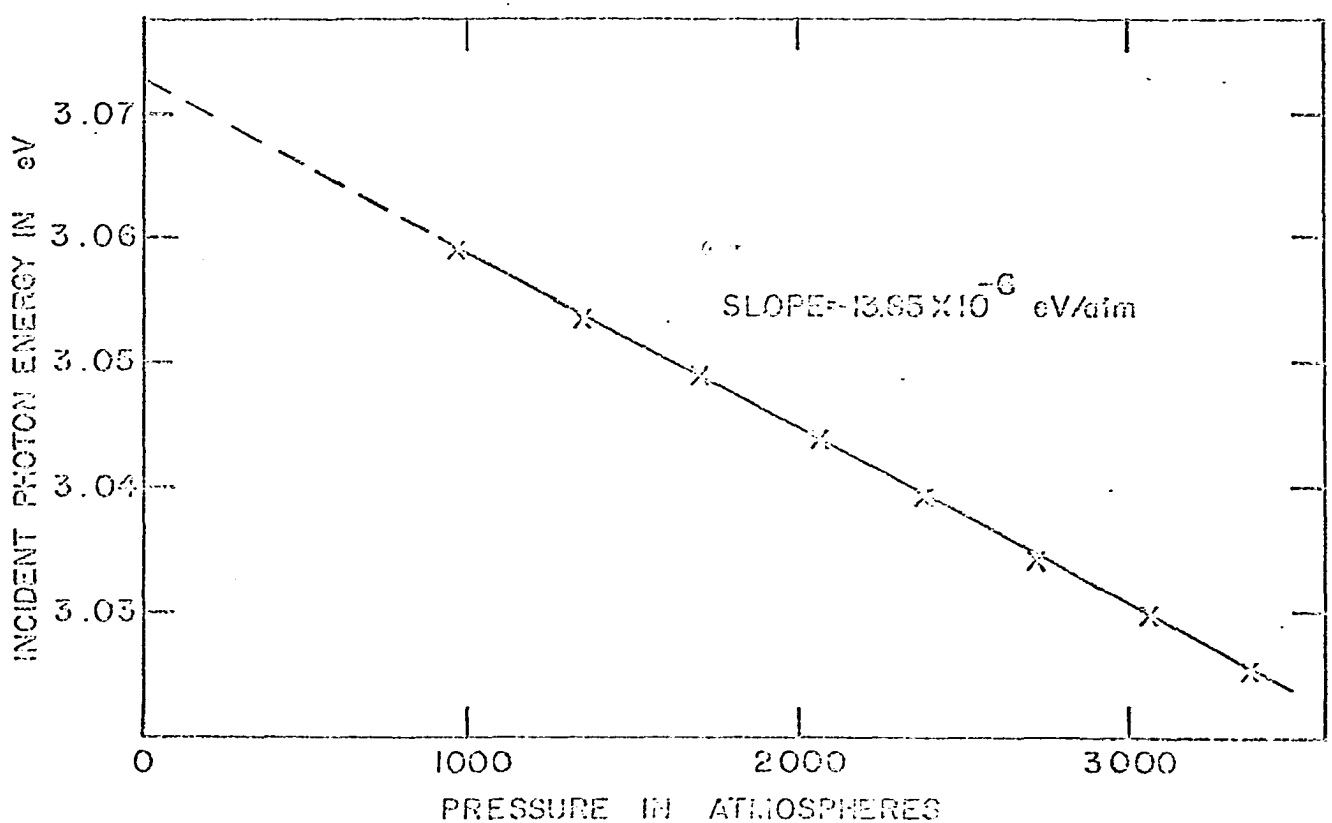

Figure 13. Typical pressure shift of the observed exciton peak in TlBr thin films

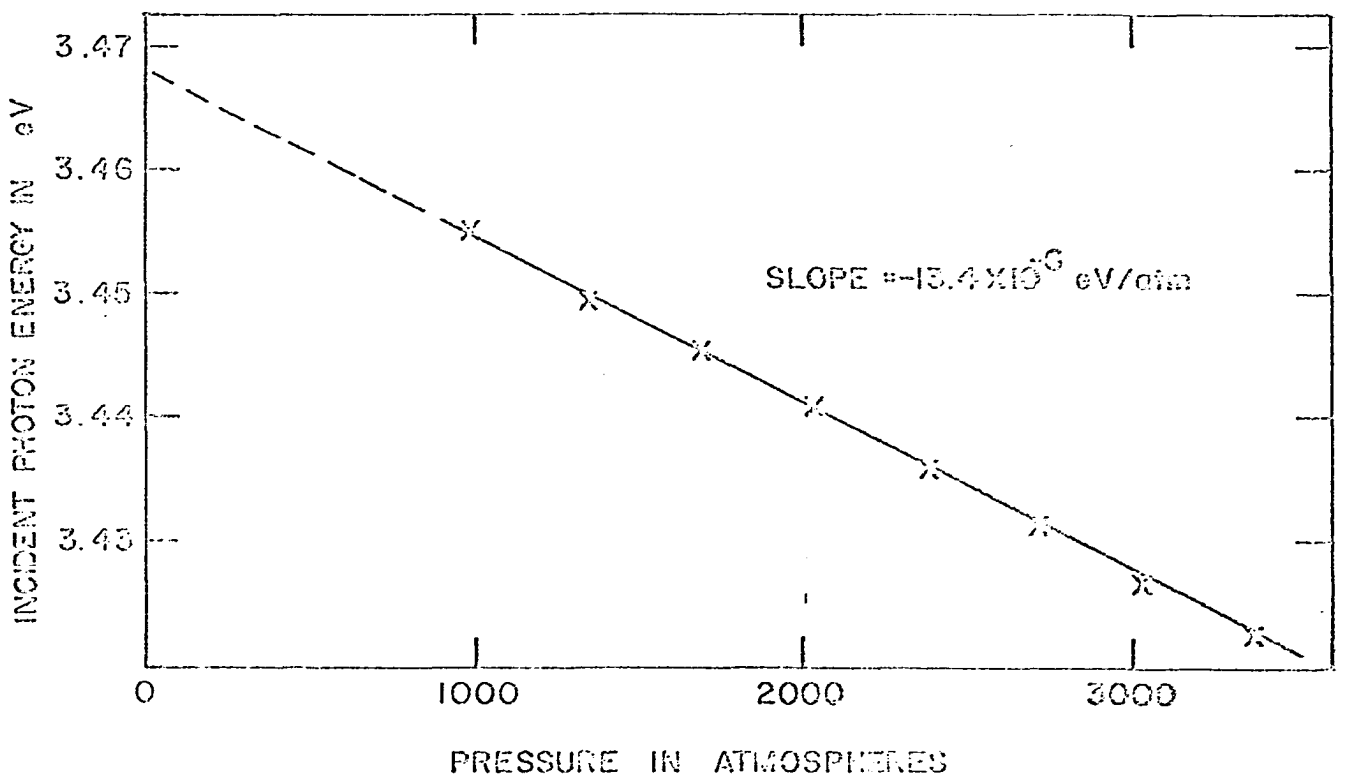

Figure 14. Typical pressure shift of the observed exciton peak in TlCl thin films

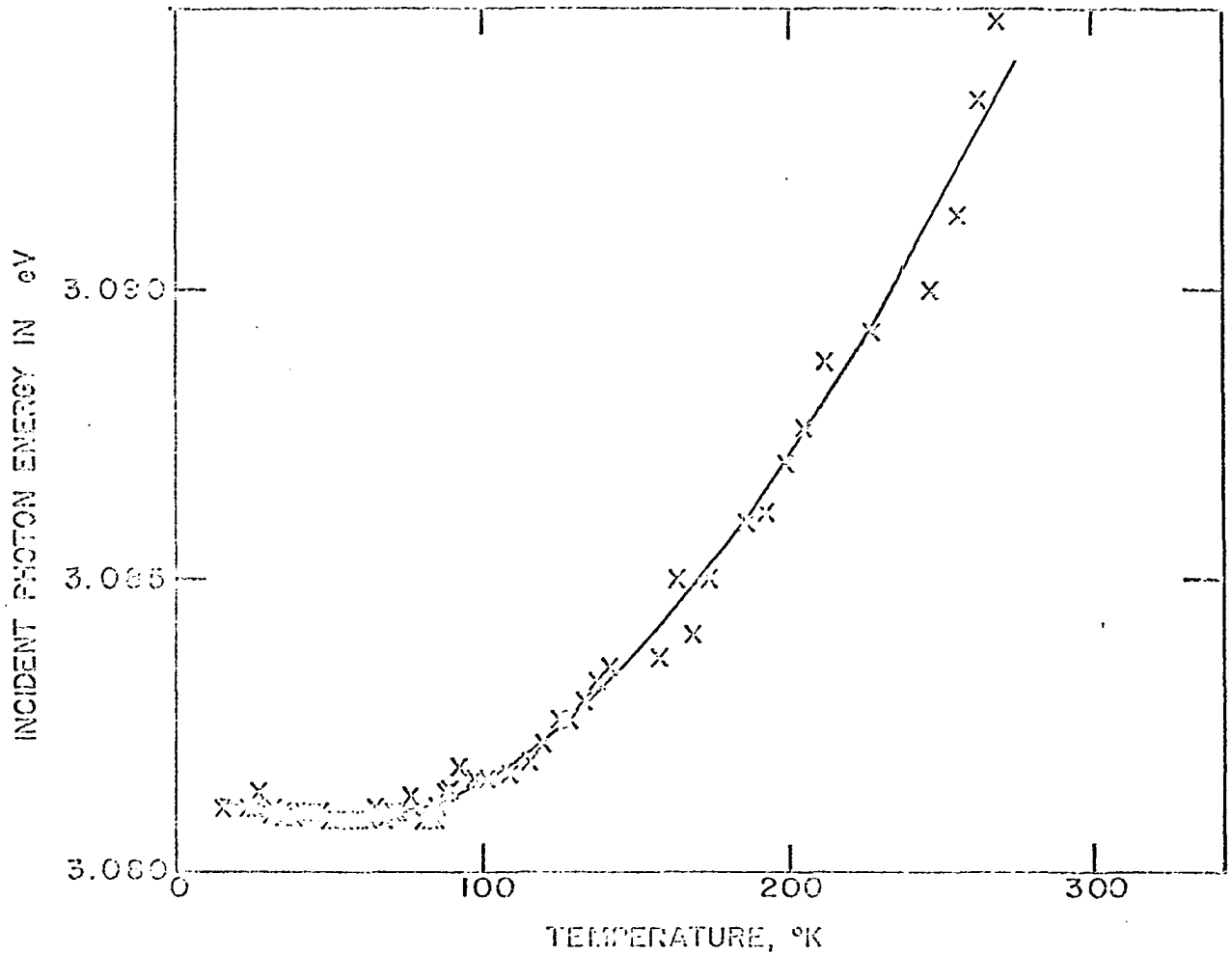

Figure 15. Temperature dependence of the exciton peak in a TlBr thin film

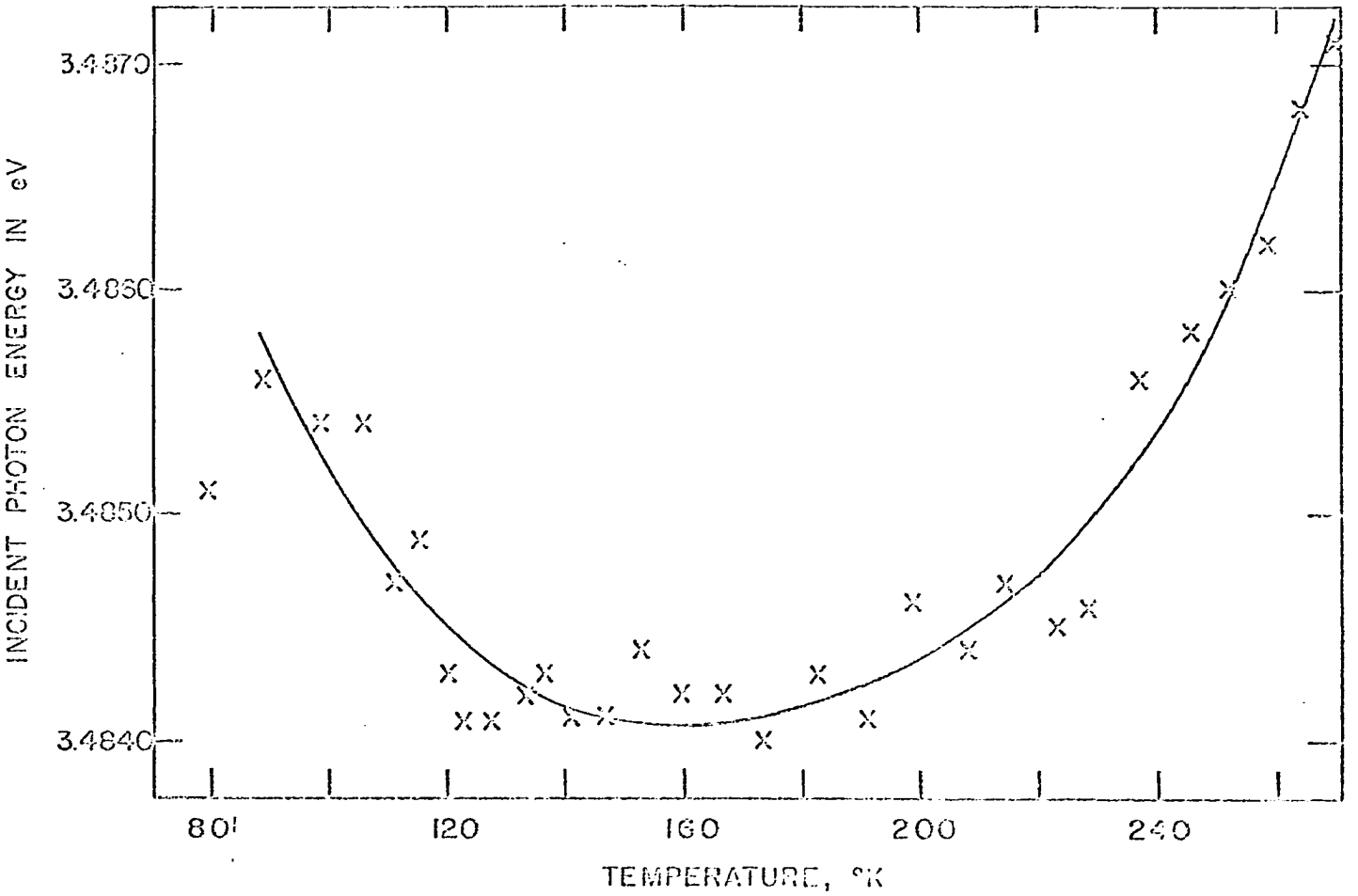

Figure 16. Temperature dependence of the exciton peak in a TlCl thin film

shape as those obtained for the exciton peak temperature shifts, but tended to have minima at lower temperatures than the curves displayed in Figures 15 and 16. At temperatures around 200°K these curves both had slopes of 3.7×10^{-4} eV/°K. For reasons that will be mentioned later these curves are not useful in interpreting the data and are not displayed.

The data displayed in Figure 17 were obtained as follows. The upper points, near absorption coefficients of 10^5 cm^{-1}, were obtained from the spectrophotometer curves of the exciton peaks of the four salts at the time their pressure shifts were measured. These data were then corrected for the large background absorption caused by the pressure cell and cryostat. The approximate absorption coefficient could then be calculated knowing the film thickness. Any increase in the reflectivity with decreasing wavelengths would shift the points obtained for the absorption coefficient of the thin films to slightly lower values. The peak positions were corrected to one atmosphere values, and plotted. The lower points are from single crystals, whose thicknesses were approximately 2 mm. It has been found that Urbach's rule is obeyed for several orders of magnitude in the absorption edges of many crystals (1, p. 128). Assuming that this is true here, the lower and upper points could be connected by a straight line on a logarithmic plot. Clearly this is not the case for AgCl, where the two points to the extreme upper left of the graph

Figure 17. Approximate absorption coefficients of single crystals (lower points) and thin films (upper points) for the four halides studied

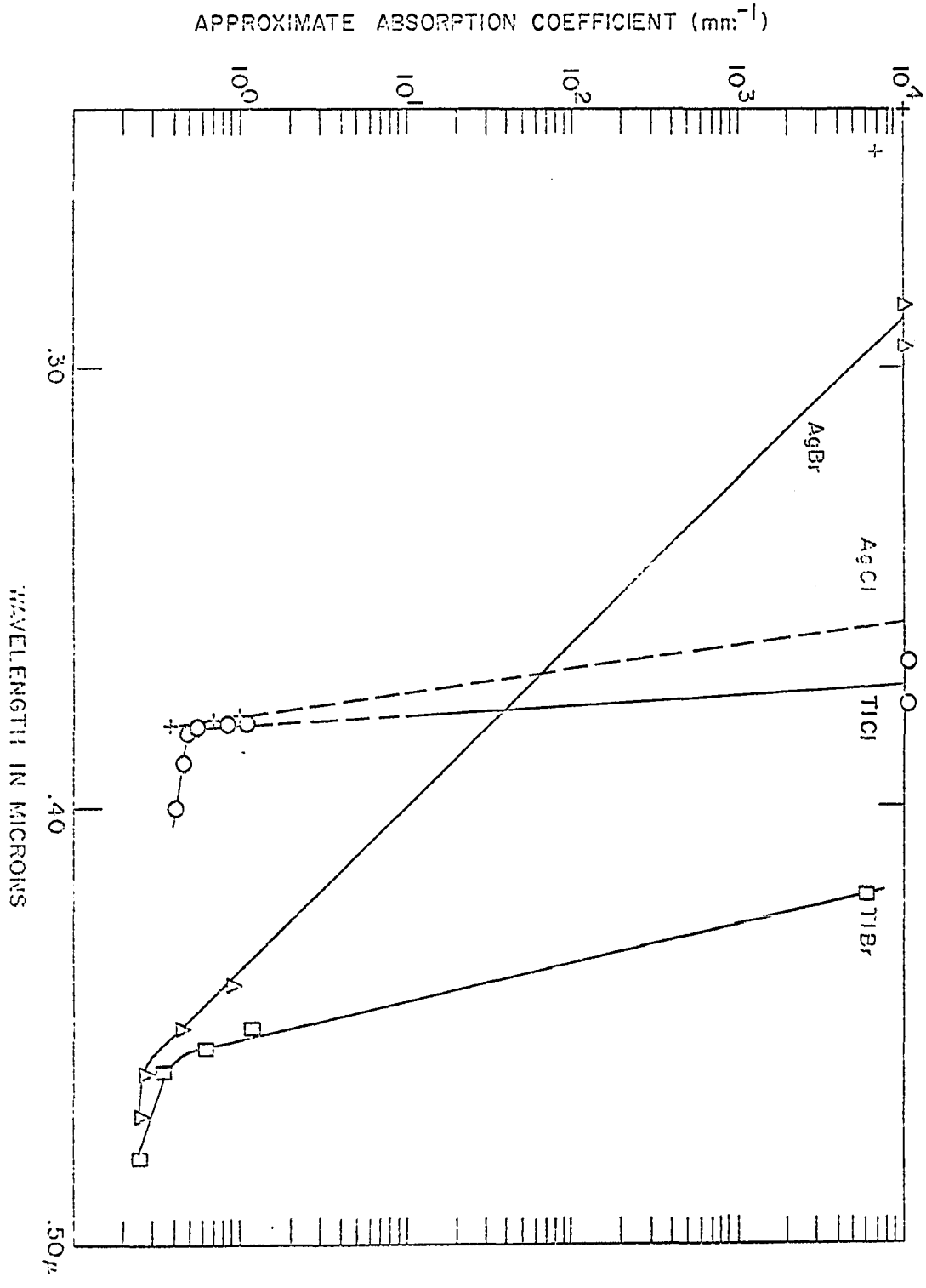
APPROXIMATE ABSORPTION COEFFICIENT (mm.$^{-1}$)
10^0
10^1
10^2
10^3
10^4
.30
.40
.50 μ
WAVELENGTH IN MICRONS
AgBr
AgCl
TlCl
TlBr

are more than 0.1 eV from a line extrapolated from the single crystal data.

The temperature dependence of the exciton peaks in AgBr and AgCl thin films was not measured since the nature of the transitions which give rise to them is well known, unlike the situation for the thallium halide excitons.

DISCUSSION

Table 3 summarizes the findings of the present work. Negative signs indicate a shift to lower energy with an increase in pressure or temperature.

Brown (14) demonstrated that the absorption edge in AgBr and AgCl is indirect. Bassani et al.(4) have pointed out that the sharp absorption peak at about 5 eV in AgCl thin films is most consistently associated with the direct exciton transition from the center of the Brillouin zone.

Referring to Figure 17, it is seen that for AgCl an Urbach plot of the absorption coefficients for single crystals and thin films cannot be connected by a straight line. The location of the exciton peak is far to the left of the line extrapolated from the single crystal data. Although the effect in AgBr is far less striking, it can be seen that here too this simple plot indicates that the single crystal absorption coefficient seems to be rising above the straight line joining these points to the thin film absorption coefficients. Since these lower points are known quite accurately, this deviation is real, even though small. These are indications that the excitons seen in the thin films are not related to the absorption edges seen in the single crystals. A description of such a system was made in the introduction using the well known example of germanium.

The pressure shifts of the edge (Table 3, row 1) and of

Table 3. Summary of pressure and temperature dependence data and calculated exciton binding energies

Measurement	Sample AgBr	AgCl	TlBr	TlCl
Pressure shift of absorption edge, in units of 10^{-6} eV/atm.	-1.9	-1.5	-16	-18
Pressure shift of exciton peak, in units of 10^{-6} eV/atm.	6.4 5.6	6.2	-13.4	-13.9
Temperature shift of absorption edge, in units of 10^{-4} eV/°K	-7.8[a]	-8.7[a]	positive[b] 3.65	positive[b] 3.67
Temperature shift of exciton peak, in units of 10^{-4} eV/°K	---	---	positive[b] 1	positive[b] 1
Pressure shift of the gap energy, in units of 10^{-6} eV/atm.[c]	---	4.8[d]	-15.8[e]	-16.7[e]
Calculated binding energy of exciton using Mannier model, in eV	0.045[f]	0.045[f]	0.065[e]	0.074[e]

[a]Values taken from Figures 6 and 7, Reference 14.

[b]Slope determined near room temperature.

[c]This quantity is determined by subtracting an estimate of the pressure dependence of the exciton binding energy from the observed exciton peak pressure shift.

[d]Reference 18.

[e]Reference 19.

[f]Reference 20.

the exciton peaks (row 2) of the silver salts have opposite signs, indicating that the quantities measured are not representing the same type of transitions (3). Assuming the exciton is a Wannier exciton, the equation

$$B(p) = \frac{1 \text{ Rydberg}}{[\epsilon_s(p)]^2} \frac{\mu^*}{m}$$

may be used to calculate the pressure dependence of the exciton binding energy. The value of μ^*/m is taken as 1/2, although this value may be less than 1/2 for direct excitons (Brown 14). The static dielectric constant, ϵ_s, has been used in the denominator. The assumption that Wannier excitons are involved is most valid for the case of indirect excitons, but may also be applied to direct excitons. In either case it is at worst an under estimate of the exciton binding energy.

Using the values of $\epsilon_s(p)$ recently measured by Jones (19) it was found that the pressure shift of the gap associated with the exciton in AgCl, found by subtracting the pressure dependence of the exciton binding energy, B(p), from the measured exciton peak pressure shift, was reduced by 23 percent (row 6). This still preserved the original opposite sign relationship between the pressure shift of the absorption edge and that of the exciton. This is further proof that the absorption edge and the edge associated with the exciton are not the same. No data for the pressure depend-

ence of the dielectric constant of AgBr are available, but it is assumed that, since the dielectric constant for AgBr is similar to the value for AgCl, the outcome of subtracting B(p) from the measured exciton pressure shift would be similar to the results obtained for AgCl.

The data in Figure 6 may be interpreted as follows. The onset of the indirect absorption edge is at $(E_g - B \pm k\theta)$. The enhancement of the edge due to the electron-hole coulomb interaction extends to energies higher than the onset of the edge by several times B, the exciton binding energy. The region of enhancement of the absorption will be pressure dependent. From Jones' (19) work it is known that the dielectric constant decreases with increasing pressure. Assuming a Wannier exciton, B(p) is proportional to ϵ^{-2}. This means that the exciton binding energy increases with increasing pressure. For the pressure range given in Figure 6, this increase would be about 5%. The measured increase of the energy range where the absorption is enhanced is about 4%.

The AgCl absorption edges displayed in Figure 7 do not exhibit the same enhancement that the AgBr curves exhibit. The reason for this likely involves the complexity of the AgCl edge compared to the AgBr edge. Brown (14) has observed four humps near the onset of the absorption edge in AgCl, generally only 0.02 to 0.03 eV apart from each other. Fassani *et al.* (4) feel that these are due to various L-type and Σ-

type transitions. Each of these transitions would have a spectrum similar to that seen in the AgBr edge, but a combination of the four spectra displaced only a few hundredths of an eV apart from one another could produce an edge which looks like those in Figure 7.

The data for the thallium salts are also enlightening. The large negative pressure shifts of the absorption edges are about equalled by the large negative pressure shifts of the exciton peaks. It is reasonable to conclude from this information that the absorption edge measured in the single crystals is the low absorption coefficient tail of the exciton band seen in the thin films.

When corrections are applied for the pressure dependence of the exciton binding energy, using the Wannier model again, the effect is to increase the observed exciton peak pressure shifts so that they nearly coincide with the corresponding values for the absorption edge shifts. The assumption that the Wannier exciton model can be used here is even more justifiable than its use for the silver salts, since the dielectric constants for the thallium salts are huge.

That the pressure shifts for the pressure dependence of the band gap corresponded more closely to the shift of the onset of the absorption edge for both thallium halides is probably a coincidence. It is likely that pressure affects the halfwidth of the exciton band slightly, so that a point

many halfwidth distances below the peak, namely near the onset of the absorption edge in single crystals, would be likely to have a slightly different pressure shift than the exciton peak.

The conclusion that the edge seen in single crystals is simply the low absorption coefficient tail of the exciton band seen in thin films is further borne out by the data in Figure 17. For both TlBr and TlCl the lower and upper sets of points are joined well by a straight line, indicating that, if Urbach's rule is obeyed, they arise from the same transition.

The slope of the absorption edge shifts rapidly with increasing temperature, but much of this shift is due to the broadening of the edge as the energy bands become thermally blurred. The shift of the edges in TlBr and TlCl was taken from the shift of points at an optical density of unity after subtracting the background absorption. This was done not only to compensate somewhat for the above effect, but also because the onset of absorption became increasingly difficult to ascertain as the temperature rose. A similar effect occurs for the exciton peak temperature shift, but is smaller in magnitude.

Zinngrebe (21) has carefully studied this effect in TlCl. He found that at temperatures above 150°K, the onset of the absorption edge shifts rapidly to longer wavelengths, while

the exciton band peak as measured in thin films shifts to the red at a much slower rate. Thus the exciton peak shift is less of an overestimate of the intrinsic edge shift with temperature than the shift at or near the onset of the absorption edge. Because of this effect, little value was attached to the measurements of the temperature shifts of the absorption edges in the single crystal samples.

The temperature shifts of the exciton peaks in TlCl and TlBr showed unusual slope reversals (see Figures 15 and 16), as did the curves obtained from the single crystal temperature dependences, but at higher temperatures. The slope above this minimum in each case was not linear, unlike the data obtained for the single crystals. By subtracting the temperature dependence of the exciton binding energy calculated from the values of $\epsilon(T)$ obtained by Samara (18), the minima of the curves tended to shift to even higher energies, since $B(T)$ was a monotonically decreasing function which raised the value of the low temperature negative slopes and lowered the values of the high temperature positive slopes. Thus the curves for the temperature dependence of the energy gaps associated with the excitons in TlBr and TlCl would appear to be rotated counterclockwise with respect to those for the temperature dependence of the exciton peaks alone and also shifted to higher energies by the amounts of the exciton binding energies, which appear in Table 3, row 6.

This procedure did not yield a straight line fit for the high temperature slope, however. Plots of the data before subtracting the temperature-dependent exciton binding energy, using various ordinates and abscissas, were likewise unsuccessful in giving a straight line slope at high temperatures. The values of $\leq 1 \times 10^{-4}$ eV/°K quoted for the exciton peak temperature shift for each thallium salt are felt to represent the upper limit of the exciton shift, and were determined at the highest temperature intervals measured to obtain the highest slope values. If the exciton and the absorption edge represent transitions involving the same direct edge, as is suggested by the data, this value also represents the upper limit of the intrinsic absorption edge shift as measured at high temperatures. Zinngrebe (21) has suggested that the much greater temperature shift of the edge is due to higher temperature transitions occurring near the foot of the absorption edge.

The temperature dependence and pressure shifts of the absorption edges and exciton peaks can be used to determine the quantity $(\partial E/\partial T)_V$ using

$$\left(\frac{\partial E}{\partial T}\right)_p = \left(\frac{\partial E}{\partial T}\right)_V - \frac{\beta\alpha}{K}\left(\frac{\partial E}{\partial P}\right)_T .$$

Here K is the isothermal compressibility and $\beta\alpha$ the volume isobaric thermal expansion coefficient. Thus the temperature shift can be broken into a portion due to thermal expansion

alone, $-3\alpha/K(\partial E/\partial P)_T$, and a portion due to lattice vibration effects, $(\partial E/\partial T)_V$. Since the absorption edge and excitons are optical manifestations of the crystal as a whole, the bulk values of α and K should be appropriate. The temperature shifts are taken at or near room temperature, and the value of $(\partial E/\partial P)_T$ at 80°K is assumed to be the same or only slightly smaller than its value at room temperature. Table 4 summarizes the results of substitution into this equation. Notice that in every case $(\partial E/\partial T)_V$ is negative, as expected (22).

Figure 16 displays the two available calculations for the band structure of AgBr. These band structures are the results of two calculations, each utilizing a different method and potential function. Bassani et al. (4) used a tight-binding method. The valence band structure was calculated, while the conduction band shape was estimated to best fit the existing data. Scop (5) carried out an augmented plane wave calculation to obtain both the valence and conduction bands. He adjusted the band structure to fit the experimental values of the direct gaps at the center of the Brillouin zones in each crystal. Only the uppermost valence band and the lowest conduction band from these calculations are shown here. The energy bands for other crystal symmetry directions were also given by Scop, but only the directions of highest symmetry, hence of highest density of states, have been shown. The Σ[(110) direction] levels have been indicated by the lines

Table 4. Calculation of $(\partial E/\partial T)_V$ for the four halides studied, using the equation

$$\left(\frac{\partial E}{\partial T}\right)_P = \left(\frac{\partial E}{\partial T}\right)_V - \frac{3\alpha}{K}\left(\frac{\partial E}{\partial P}\right)_T$$

Crystal	$3\alpha/K$ atm/°K	$(\partial E/\partial P)_T$ x10^{-6}eV/atm	$3\alpha/K(\partial E/\partial P)_T$ x10^{-4} eV/°K	$(\partial E/\partial T)_P$ x10^{-4} eV/°K	$(\partial E/\partial T)_V$ x10^{-4} eV/°K
AgBr[a]	44.5[b]	-1.5[c]	-0.67	-7.8[c]	-8.5
AgCl[a]	39.2	-1.9[c]	-0.74	-8.7[c]	-9.5
TlBr[d]	34.0[e]	-15.8[f]	-5.37	1[f]	-4.4 to -5.4
TlCl[d]	37.0[e]	-16.7[f]	-6.18	1[f]	-5.2 to -6.2

[a]Indirect absorption edge.

[b]Calculated from values of C_{11}, C_{12}, and C_{44} from Reference 23.

[c]Reference 14.

[d]Direct absorption edge.

[e]Reference 11.

[f]Data from Table 3.

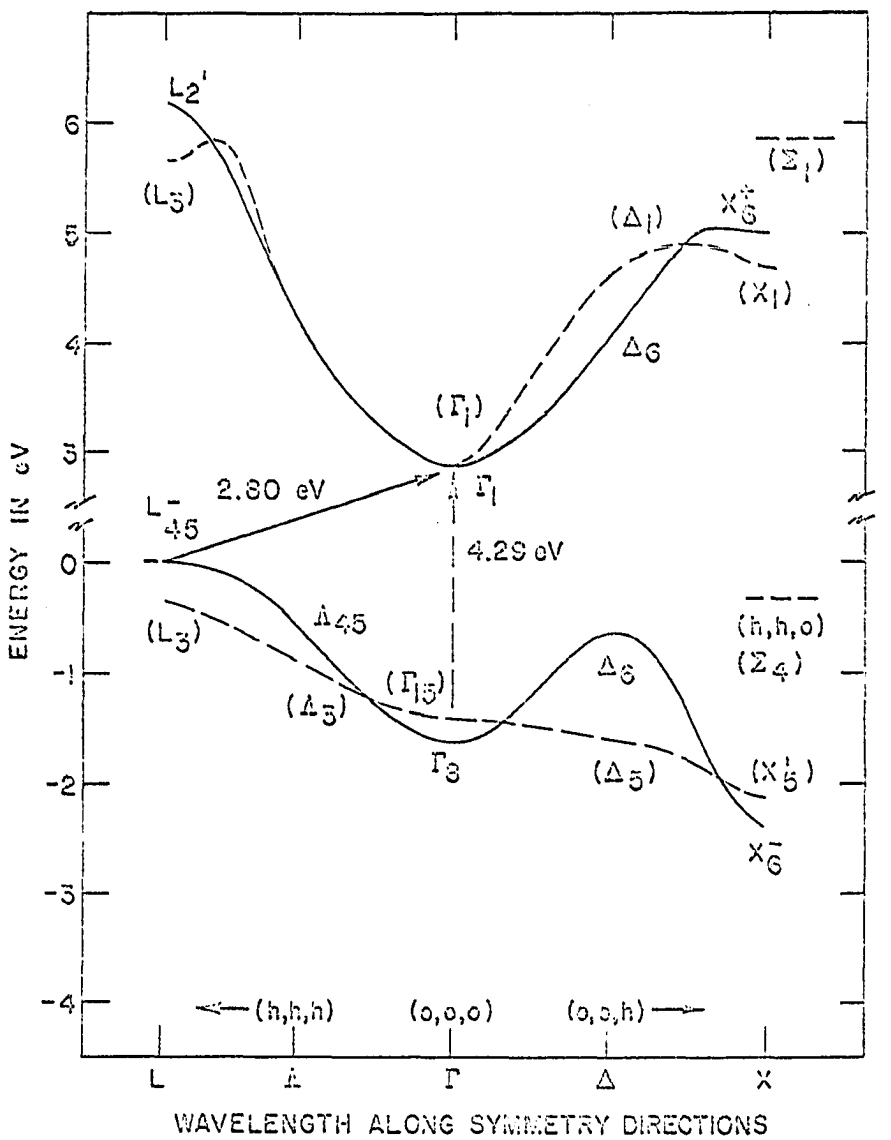

Figure 18. Band structure calculations for AgBr, Bassani et al. (4) (solid lines) and Scop (5) (dashed lines)

to the right of the main band structure diagram. The two conduction band minima were superimposed graphically to have a common minimum, while the valence bands were adjusted as follows. The indirect edge ($L_{4,5}^{-}$ to Γ_1^{-}) was adjusted to fit the experimental value (2.80 eV) for Bassani's bands, whereas the direct edge transition (Γ_{15}^{-} to Γ_1^{-}) was made to fit the experimental value (4.29 eV, as given by Scop) for Scop's bands. This was in keeping with the original adjusting methods of Bassani and Scop. The solid lines are those corresponding to Bassani's band structure, while the dashed lines are those of Scop's calculations.

Table 5 contains the energies for direct transitions from the various valence band maxima to the conduction band. These figures are only approximate, and are given in the notation used by Bassani.

Table 5. Energies of the direct transitions from the valence band maxima in AgBr

Transition	Bassani, et al. (4)	Scop (5)
Γ_{15} to Γ_1	4.5 eV	4.29 eV
Δ_6 to Δ_6	4.75 eV	----
$L_{4,5}^{'}$ to $L_2^{'}$	6.15 eV	6.0 eV
Σ_4 to Σ_1	----	6.0 eV

Figure 19 displays the corresponding band structure for AgCl. The same description as for Figure 18 applies, except that the indirect transition, thought to correspond to the indirect absorption edge (L_3' to Γ_1), has an energy of 3.22 eV (4), while the direct transition at the Brillouin zone center has the value 5.13 eV (5). Table 6 is a summary of the direct transition energies from the various valence band maxima in Figure 19.

Table 6. Energies of the direct transitions from the valence band maxima in AgCl

Transition	Bassani et al. (4)	Scop (5)
Γ_{15} to Γ_1	5.45 eV	5.13 eV
Δ_1 to Δ_1	4.40 eV	5.70 eV
L_3' to L_2'	6.30 eV	7.10 eV
Σ_4 to Σ_1	---	6.65 eV

Sketches of the absorption edges of thin films of AgBr and AgCl appear in Figure 20. The energies of the transitions from Tables 5 and 6 are shown as solid arrows (Bassani) and dashed arrows (Scop). Looking at Figure 20a, we see that the two values of Γ_{15} are quite near the high energy valley associated with the first exciton peak seen. If this exciton is due to a direct transition, it should appear at $E_g - B$. Thus the distance from the valley to the peak represents the exciton binding energy, B, while the energy of the gap related to the

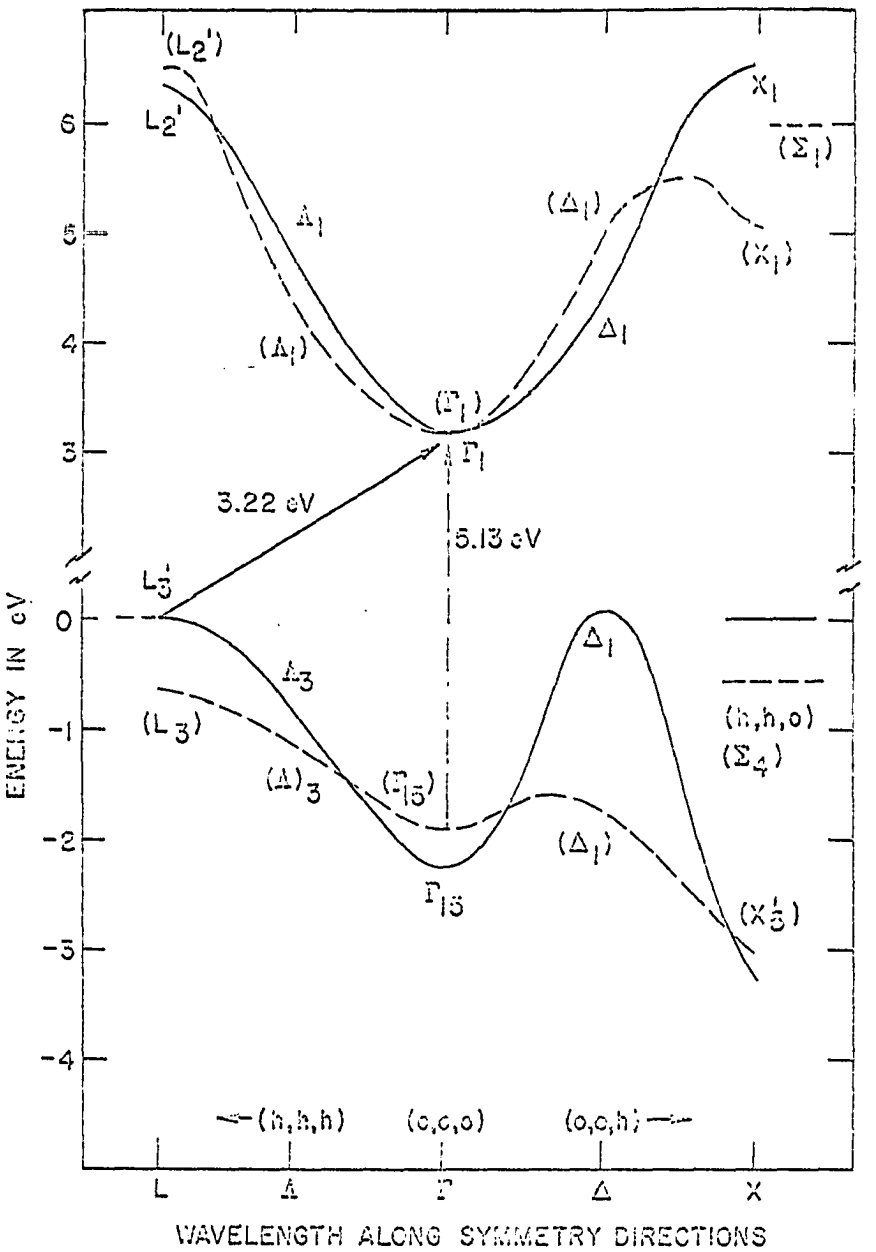

Figure 19. Band structure calculations for AgCl; Bassani et al. (4) (solid lines) and Scop (5) (dashed lines)

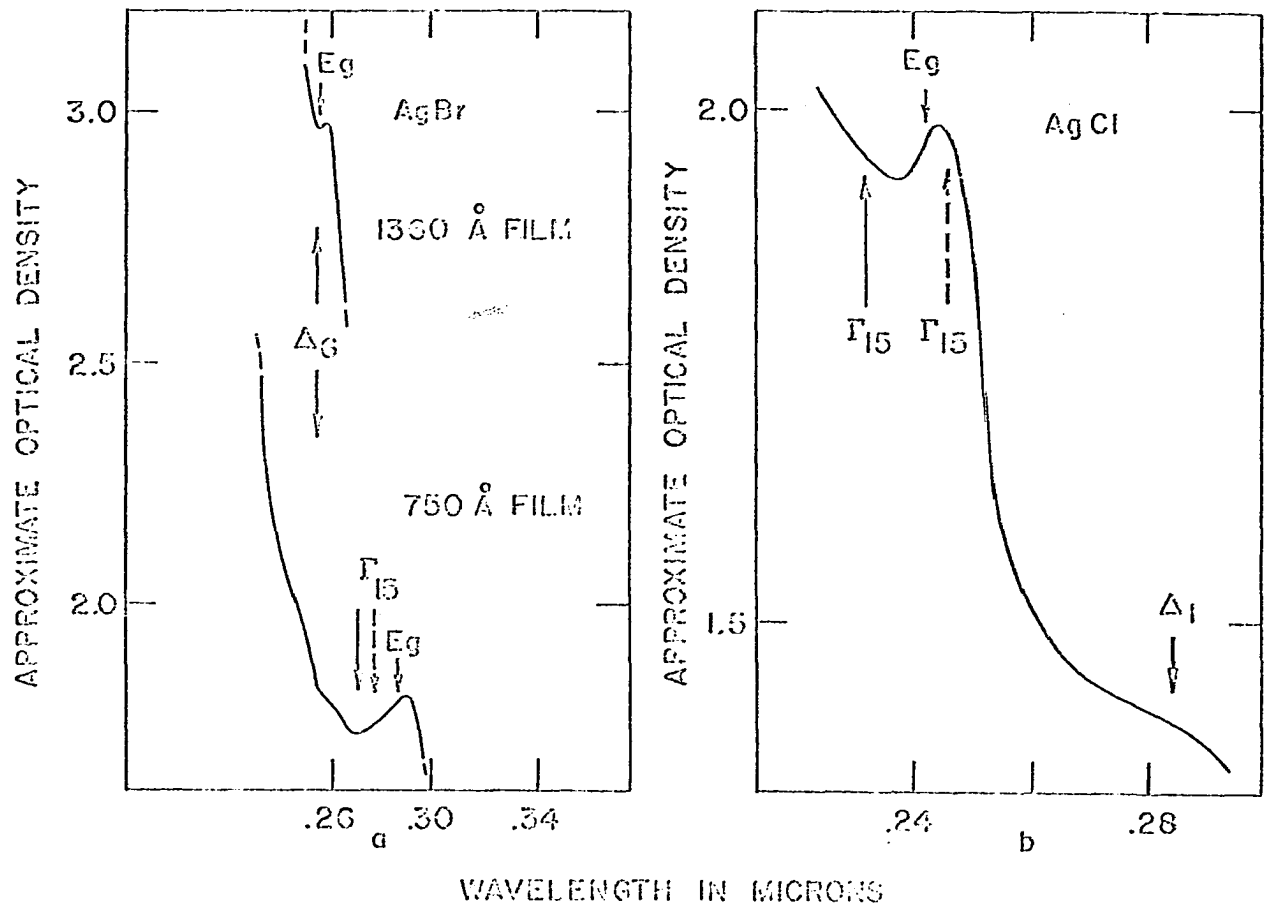

Figure 20. Location of calculated transitions on sections of the AgBr and AgCl thin film absorption edges

exciton is E_g. The transition Δ_6 points to a hump in the structure of the thin film which is resolved in the thicker film. Because of the location of the Δ_6 transition on the energy band structure, it should appear as a weak peak at best, since the density of states is low. Probably this hump is due to spin orbit splitting of the direct Γ transition, which was not included in either band structure calculation. The small arrows to the left of the exciton peaks in Figure 20 represent the position of the direct edge energy gaps calculated by subtracting the exciton binding energies from the measured exciton peak positions, assuming Wannier excitons are involved with effective masses of 0.5. These energies are tabulated in Table 3, row 6. That the arrows indicating the transitions in Figure 20 do not all coincide nor all point to logical positions for an energy gap location is an indication of the uncertainty in the band structure calculations.

It is not clear what dielectric constants should be used to calculate the direct exciton binding energy. Values of the optical dielectric constant (14), the static dielectric constant[1], and some intermediate value between these (24) have been suggested. The values used here are for the static dielectric constants, which give at worst an underestimate of the exciton binding energy.

---

[1]Lynch, D. W., Ames, Iowa. Data from F. C. Brown, Urbana, Illinois, University of Illinois, Physics Department. Private communication. 1967.

The spectrum in Figure 20b represents the absorption edge of a thin film of AgCl near the exciton peak. The two energies calculated for the Γ_{15} to Γ_1 transition straddle the experimental location for the direct gap energy. Again the binding energy was estimated using a Wannier model exciton. Both here and for the two exciton peaks in the AgBr film, this value falls short of the experimental value which may be estimated from the energy which separates the exciton peak from the high energy valley nearby. The extent of this discrepancy is an indication of the degree to which the excitons involved are different from ideal Wannier excitons.

Sketches of the portions of the absorption edges near the exciton peaks in TlBr and TlCl are given in Figures 21a and 21b, respectively. Assuming that the excitons are direct Wannier excitons, the energy gaps have been calculated (Table 3, row 6). These appear as arrows pointing to the short wavelength valleys associated with the exciton peaks. The agreement of the calculated energy gaps and the measured gaps is excellent, indicating that the Wannier model described these excitons well. This is in agreement with the assumptions made in the Wannier model, since the dielectric constants of TlBr and TlCl are very high.

The results of Slykhouse and Drickamer (25) and Zahner and Drickamer (26) may be interpreted in the light of the data taken in this work. Slykhouse and Drickamer measured the

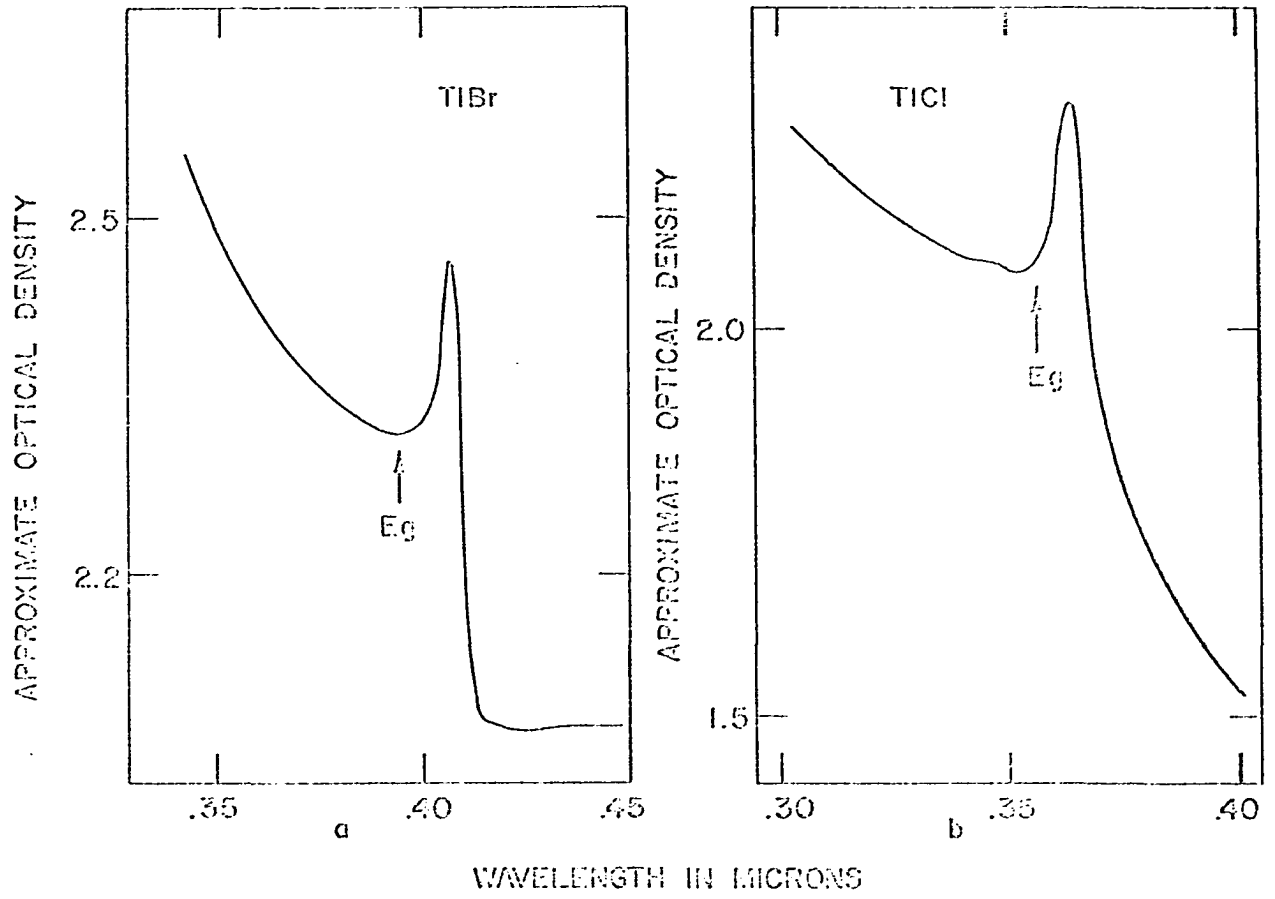

Figure 21. Location of calculated transitions on sections of the TlBr and TlCl thin film absorption edges

pressure shift of the absorption edge in the silver halides to very high pressures. In the pressure range used in this work, their values for the edge shifts were -3×10^{-7} eV/atm and -6×10^{-7} eV/atm for AgBr and AgCl respectively. These values are both only a fraction of the values of the shifts observed in this work at the onset of the absorption edge, but this can be readily explained since their measurements were not made at the onset of the edge. The farther away from the onset of the absorption edge the measurements are made, the more effect the pressure shift of the direct edge, which is of opposite sign, will have on the net pressure shift of the edge.

SUMMARY AND CONCLUSIONS

The silver halide absorption edges have been extensively studied, and it has been generally accepted that for both AgBr and AgCl, the edge seen in the single crystals is indirect, with direct excitonic transitions apparent in thin film spectra superimposed upon this indirect edge. The band structure calculations have not been able to determine which of the several valence band maxima are responsible for these indirect transitions. Bassani et al. (4) suggested that either the L_3 to Γ_{15} or the Σ_4 to Γ_{15} transition could account for these spectra, while Scop (5) indicated that the transition is the L_3 to Γ_{15}. From the results of this work, it can be concluded that whichever valence band maximum is involved, it is likely the same for both AgBr and AgCl. This conclusion is reached when the implications arising from the nearly identical pressure shifts of the indirect absorption edges in the two halides are considered. The complicated band structure for these halides arises from the overlapping of the many silver p and halogen d states. Since the symmetry properties at Σ and L are quite different, one would expect much different pressure dependences of transitions originating from these points to result (3). Since this is not so, the transitions are thought to arise from the same symmetry locations in both AgBr and AgCl.

Using ultrasonic excitation of uniaxial strain, Ascarelli

(27) has found that the valence band maximum in the (111) direction (L-symmetry) is responsible for the indirect transition in AgBr. Thus from the above argument, it may be asserted that the L to Γ transition is responsible for the indirect absorption edge in both AgBr and AgCl.

Knox (28) has pointed out that the 5 eV excitonic transition in AgCl is anomalous, since a spin-orbit splitting of at least 0.1 eV is expected, while a splitting of only 0.05 eV is observed. For AgBr, the spin-orbit splitting is observed to be about 0.6 eV, which is close to the expected value. This appears as the two peaks at 2900 Å and 2600 Å in Figure 20a, which have understandably nearly the same pressure shifts as measured in this work.

The results for the thallium halides are quite consistent. They all imply a direct edge which is the low absorption coefficient tail of the direct exciton band seen in the thin films. These results are consistent with the findings of Makita et al. (29) who have determined from magnetoresistance measurements that the valence band in TlCl is spherical and located at zero wave vector. Tamura and Masumi (30) and Hodby et al. (24) have measured the cyclotron resonance of TlCl single crystals and found that these measurements indicate a simple conduction band with its minimum at zero wave vector. Further indication that the exciton peak and the absorption edge seen in single crystals are manifestations of the same,

direct transition in the thallium halides is the similarity in their temperature dependences.

From Table 4 we see that the value of $(\partial E/\partial T)_\gamma$ for the thallium halides is negative and therefore not anomalous, even though the temperature dependence of the absorption edge in these halides is anomalous.

LITERATURE CITED

1. Dexter, D. L. and R. S. Knox. Excitons. New York, New York, Interscience Publishers. 1965.

2. McLean, T. P. Excitons in Germanium. In Kuper, C. G. and G. D. Whitfield, eds. Polarons and Excitons. pp. 367-375. New York, New York, Plenum Press. 1962.

3. Paul, William. Band Structure of the Intermetallic Semiconductors from Pressure Experiments. Journal of Applied Physics 32: 2082. 1961.

4. Bassani, F., R. S. Knox, and W. Beall Fowler. Band Structure and Electronic Properties of AgCl and AgBr. Physical Review 137: A1217. 1965.

5. Scop, Peter M. Band Structure of Silver Chloride and Silver Bromide. Physical Review 139: A934. 1965.

6. Brothers, A. D. The Effect of Pressure on F Center Luminescence. Unpublished M.S. thesis. Ames, Iowa, Library, Iowa State University. 1965.

7. Bridgeman, P. W. The Physics of High Pressure. London, England, G. Bell and Sons, Ltd. 1949.

8. Finnemore, D. K., J. E. Ostenson, and T. F. Stromberg. Secondary Thermometer for the 4 to 20°K Range. Review of Scientific Instruments 36: 1369. 1965.

9. Heavens, O. S. Optical Properties of Thin Solid Films. New York, New York, Dover Publications, Inc. 1965.

10. Dugdale, J. S. The Equation of State of Solid Helium. Nouvo Cimento 9 Supplement 1: 27. 1958.

11. Ballard, Stanley S., Kathryn A. McCarthy, and William L. Wolfe, eds. Optical Materials for Infrared Instrumentation. Ann Arbor, Michigan, Physics Department, University of Michigan. 1959.

12. Hodgman, Charles D., ed. Handbook of Chemistry and Physics. Forty-First Edition. Cleveland, Ohio, Chemical Rubber Publishing Company. 1960.

13. Zallen, R. The Effect of Pressure on Optical Properties of the Noble Metals. In F. Abeles, ed. Optical Properties and Electronic Structure of Metals and Alloys.

pp. 164-174. Amsterdam, Netherlands, North-Holland Publishing Company. 1966.

14. Brown, Frederick C. Electronic Properties and Band Structure of the Silver Halides. Journal of Physical Chemistry 66: 2368. 1962.

15. Brown, F. C., T. Masumi, and H. H. Tippins. Fine Structure in the Absorption Edge of the Silver Halides. Journal of the Physics and Chemistry of Solids 22: 101. 1961.

16. Smith, R. A. Semiconductors. Cambridge, England, Cambridge University Press. 1959.

17. Urbach, F. The Long Wavelength Edge of Photographic Sensitivity and of the Electronic Absorption of Solids. Physical Review 92: 1324. 1953.

18. Jones, B. W. The Dielectric Constant of Ionic Solids and Its Change with Hydrostatic Pressure. Philosophical Magazine 16: 1085. 1967.

19. Samara, G. A. Temperature and Pressure Dependence of the Dielectric Constants of the Thallous Halides. Physical Review 165: 959. 1968.

20. Smith, G. C. Luminescence and Photoconductivity in Silver Halides. Unpublished Ph.D. thesis. Ithaca, New York, Library, Cornell University. 1965.

21. Zinngrebe, Horst. Die Optische Absorption von Thalliumchlorid. Zeitschrift für Physik 154: 495. 1959.

22. Fan, H. Y. Temperature Dependence of the Energy Gap in Semiconductors. Physical Review 82: 900. 1951.

23. Tannhauser, D. S., L. J. Bonner, and A. W. Lawson. Temperature Variation of the Elastic Constants of AgBr. Physical Review 102: 1276. 1956.

24. Hodby, J. W., J. A. Borders, F. C. Brown, and S. Foner. Cyclotron Resonance of the Polaron in KCl, KBr, KI, RbCl, AgCl, AgBr, and TlCl. Physical Review Letters 19: 952. 1967.

25. Slykhouse, T. E. and H. G. Drickamer. The Effect of Pressure on the Absorption Edge in Silver Halides. Journal of the Physics and Chemistry of Solids 7: 207. 1958.

26. Zahner, J. C. and H. G. Drickamer. The Effect of Pressure on the Absorption Edge in Heavy-Metal Halides. Journal of the Physics and Chemistry of Solids 11: 92. 1959.

27. Ascarelli, G. Experimental Detection of Internal Polaron States Associated with the Indirect Edge of AgBr Using Piezo-Optical Transmission. Physical Review Letters 20: 44. 1968.

28. Knox, R. S. and N. Inchauspé. Exciton States in Ionic Crystals. Physical Review 116: 1093. 1959.

29. Nakita, Yunosuke, Koichi Kobayashi, and Mihoko Kanada. Valence Band from the Transient Magnetoresistance of Holes in TlCl. Journal of the Physical Society of Japan 23: 1180. 1967.

30. Tamura, Hiroshi and Tatsuo Masumi. Observation of Cyclotron Resonance in TlCl. Journal of the Physical Society of Japan 23: 1173. 1967.

ACKNOWLEDGEMENTS

I wish to express my greatest appreciation to Dr. D. W. Lynch for his guidance in every phase of this work, without which it would not have been possible to complete. My thanks go to Dr. R. M. Morgan for his assistance and knowledge in preparing the thin film samples. For the extremely pure samples of AgBr and AgCl I thank Dr. R. S. Van Heyningen. For advice on the design of the pressure equipment and for the construction of the apparatus I thank Dr. C. S. Swenson, Mr. Dean D. Woods, and Mr. E. Russell Clark.